Research on Engineering Structures & Materials
www.jresm.org
MIM Research Group

Research Article

Flexural response of GFRP-reinforced BubbleDeck biaxial voided slabs under monotonic and repeated loading

Ahmed A. Mohammed Ali [*,a], Suhaib Y. Al-Darzi [b]

Department of Civil Engineering, College of Engineering, University of Mosul, Mosul, Iraq

Article Info

Article History:

Received 11 May 2026

Accepted 06 June 2026

Keywords:

BubbleDeck slabs;
Diaphragm reinforcement;
Finite element analysis;
GFRP reinforcement;
Repeated loading

Abstract

An essential requirement for today's building is to provide long spans with minimizing the weight of concrete for sustainability objectives. A viable option that has evolved is biaxial voided (BubbleDeck) slabs, which reduce concrete weight while preserving structural efficiency. This study analyses the structural behavior of GFRP-reinforced biaxial voided slabs through experimental and numerical investigations. A concentrated load was exerted on twelve slabs. The testing parameters were reinforcement type, diaphragm reinforcement, voids diameter, and loading procedure. Experimental results indicate that slabs with steel reinforcement exhibit superior stiffness and enhanced ultimate load capacity compared to GFRP slabs. The deformability and energy absorption of GFRP slabs were significantly greater. Experimental results showed that the steel-reinforced control slab achieved an ultimate load of 224.2 kN, whereas the GFRP-reinforced ribbed slab showed a 46.3% lower capacity and approximately 4.4 times greater maximum deflection. Under repeated loading, the specimens exhibited progressive stiffness degradation and crack widening while preserving stable flexural behavior throughout the loading cycles. Furthermore, the diaphragm reinforcement arrangement provided the most efficient load-transfer mechanism and superior structural performance. Meanwhile, the smaller void configuration enhanced energy absorption and deformability, demonstrating the important role of void geometry in slab behavior. To further examine the structural response, a nonlinear finite element simulation model was developed by ABAQUS/CAE. The numerical model showed reasonable agreement with the experimental observations, with deviations ranging from 3.0% to 15.2% for ultimate load and deflection predictions. Moreover, a parametric evaluation was carried out, revealing that higher concrete compressive strength plays a key role in improving the overall structural performance of the slab system. The research indicates that BubbleDeck slabs can be fortified with GFRP, rendering them a more efficient and sustainable substitute for reinforced concrete slabs.

1. Introduction

With the rapid advancement in modern construction, the need for structural systems that can offer longer spans, less material consumption, and better sustainability has been growing rapidly. Solid reinforced concrete slabs, however, constitute a notable percentage of the total structural weight of the buildings, thereby increasing the foundation loads and the overall cost of the construction. This has led to the development of a wide range of research towards lightweight slab systems that can reduce the concrete quantity while providing sufficient structural performance. Among the different options, the biaxial voided slab system known as the BubbleDeck slab is a feasible alternative.

*Corresponding author: a.aldubony@uomosul.edu.iq
[a]orcid.org/0000-0003-0172-0416; [b] orcid.org/0000-0001-5346-8836
DOI: http://dx.doi.org/10.17515/resm2026-1670me0511rs

BubbleDeck slabs use spherical void formers inside the slab depth to remove concrete from areas with low contribution to structural resistance. The technology is capable of reducing the self-weight by roughly 30-35 % by eliminating concrete in the vicinity of the neutral axis, while ensuring acceptable stiffness and flexural load carrying capacity. Previous investigations have demonstrated that the structural behavior of biaxial voided slabs is dominated mainly by the two-way bending action with the concrete ribs created between the voids functioning as the dominant load transfer elements. [1-6]. Experimental and numerical analyses have shown that the system is capable to realize material savings and structural efficiency improvements with no substantial loss of structural performance [7,8]. Furthermore, the experimental results revealed that the crack pattern of voided slabs closely resembles that of solid slabs. In two-way slabs, flexural cracking generally initiates at the slab center and propagates radially toward the supports with increasing load [9].

Simultaneously with the advancement of lightweight slab systems, Fiber-reinforced polymer (FRP) bars have gained increasing attention as reinforcement materials in concrete structures. Compared to traditional steel reinforcement, the FRP reinforcement has many benefits, such as high corrosion resistances, high tensile strength, electromagnetically neutralities, and light weights [10]. These properties make FRP reinforcement especially beneficial for structures confronted with aggressive environmental conditions such as marine infrastructure, bridge decks, coastal structures [11-13]. Among the various FRP reinforcement types, GFRP (Glass fiber-reinforced polymer) bars have attracted considerable research interest and have become one of the most commonly adopted reinforcement alternatives due to their favorable mechanical performance and durability properties. Much experimental research has been conducted on the behavior of concrete element with GFRP bars. This research firmly shows that, generally, concrete GFRP reinforced member has larger deflections and wider crack spacing when compared to its steel counterpart due to the relatively low modulus of elasticity of reinforcement [14-17]. However, it should be noted that superior corrosion resistance and durability of GFRP reinforcement may increase the service life of reinforced concrete structures greatly, especially when exposed to aggressive environments.

There have been many studies on FRP RC beams and slabs but very few on the application of GFRP bars for the novel biaxial voided slab systems. Mtashar and Al-Azzawi [18] investigated the behavior of two-way voided reinforced concrete slabs strengthened with GFRP sheets under monotonic and repeated loading through experimental testing and ABAQUS finite element modeling. The results showed that voids reduced load capacity and increased deflection, while repeated loading caused additional stiffness degradation and damage accumulation. GFRP strengthening significantly improved structural performance, increasing the ultimate load by up to 20% and reducing deflection. The geometric shape of voided slabs alters the mechanical properties of GFRP reinforcement, and this adds more complexity in the structural behavior like stiffness degradation, cracking development and the ultimate load capacity.

Recent studies have investigated the performance of reinforced concrete and GFRP-reinforced elements under cyclic loading. Sidhardhan and Madasamy [19] observed stiffness loss and higher deformation of GFRP-reinforced slabs when subjected to cyclic loading while Al-Shaarbaf et al. [20] observed similar effects on voided concrete slab strips. However, there is little information on the performance of GFRP reinforced BubbleDeck slabs under repeated loading. Therefore, the cumulative effect of internal voids and GFRP reinforcement on stiffness deterioration, crack propagation and energy dissipation needs to be investigated further. Moreover, effects of some parameters such as diaphragm reinforcement and void pattern on the performance of GFRP reinforced BubbleDeck slabs are still not fully studied in the literature.

Although numerous studies have been conducted on both BubbleDeck slab technique, a substantial gap of research exists on the structural response of GFRP reinforced BubbleDeck slabs. As well as diaphragm reinforcement is introduced in concrete slabs to enhance force transfer between adjacent concrete parts and improve the distribution of internal stresses around the voided regions. It also contributes to improving the integrity of the slab system in critical loading zones and reducing stress concentrations caused by the discontinuity introduced by the spherical voids.

On the other hand, the interaction effects of reinforcement type, void geometry and diaphragm reinforcement under repeated loading have been hardly investigated so far. In addition, the validation of numerical models by experimental data for this category of structural system is yet to be widely recognized.

Thus, this study presents a combined experimental and numerical study on the structural response of GFRP reinforced BubbleDeck slabs. A total of twelve slabs with overall dimensions of 2000×2000×200 mm was built and tested with central concentrated load. The experimental program was developed to study the effects of several relevant parameters such as reinforcement type (steel and GFRP), load type (monotonic and repeated loading), void diameter, diaphragm reinforcement. Besides the experimental study, nonlinear finite element analyses were performed by using ABAQUS/CAE with employing the Concrete Damaged Plasticity model to reproduce the structural behavior of the tested slabs [21,22]. The numerical models were validated against experimental results based on load-deflection response, crack patterns and reinforcement strain. The numerical model was then utilized for parametric study to explore the effects of diaphragm reinforcement ratio and concrete compressive strength on the slab behavior. The results of the present study offer a good understanding of the performance of GFRP-reinforced biaxial voided slab systems and can lead to novel, lightweight, sustainable and durable structural solutions for contemporary RC construction.

2. Experimental Procedure

2.1. Material Characteristics

2.1.1. Concrete Composition

Based on previous work by the authors (Mohammed Ali & Al-Darzi) [23] Normal-strength concrete (NSC) was designed to attain a 28-day compressive strength of 25 MPa. The concrete mix preparation based on (ACI 211.1) [24] is shown in Table 1. Ordinary Portland Cement was used and it was produced by the Badosh Cement Company in this research. The tests and analysis were carried out according to the requirements of IQS NO.5 (Iraqi Standard Specification, 2018) [25]. The fine aggregate is natural river sand that conforms to grading requirements of BS 882 [26] with maximum size of 4.75 mm. Rounded Natural aggregate with a maximum size of 10mm were used alongside coarse gravel. It is sourced from the Tigris River (Mosul, Iraq), that we obtain this gravel. The experimental result for the average strength of the cylinder at 28 days is 27.8 MPa. The measured slump values ranged from 143 to 164 mm, indicating adequate workability for all concrete batches in accordance with ASTM C143/C143M [27].

Table 1. Mix design of concrete

Cement (kg/m^3)	Fine Aggregate (kg/m^3)	Coarse Aggregate (kg/m^3)	Water (kg/m^3)	fc' (MPa)
450	860	950	170	27.8

2.1.2. Reinforcement

Bars of GFRP with nominal diameters 8, 10 and 16 (mm) were used. The mechanical properties were evaluated by tensile test (ASTM D7205/D7957) [28,29], reported in Table 2. The conventional reinforcement bars with nominal diameter 8, 10 and 16 (mm) were used as reference, this steel reinforcement exhibited modulus of elasticity of 200 GPa.

The steel and GFRP reinforcing bars used in this study were obtained from local commercial suppliers in Mosul, Iraq. The GFRP bars were manufactured with a helically-wrapped surface profile to improve bond performance and mechanical interlock with the adjacent concrete. Before specimen manufacturing, representative samples of both reinforcement types were tested in tension to check the reproducibility of the material properties used, and the measured mechanical parameters are listed in Table 2.

Table 2. Mechanical Properties of Steel and GFRP bars

Reinforcement Type	Diameter (mm)	Area (mm^2)	Yield Stress (MPa)	Tensile Strength (MPa)	Ultimate Strain (%)	Elastic Modulus (GPa)
Steel	8	50.24	422	628	17.0	200
	10	78.50	541	637	15.0	200
	16	201.0	595	686	16.0	200
GFRP	8	50.24	N/A	1223	2.18	55
	10	78.50	N/A	1108	2.08	53
	16	201.0	N/A	917	1.80	50

2.1.3. Void Formers

The void formers consisted of commercially available PVC hollow spheres with diameters of 94 and 125 mm. The good chemical resistance and the long lifetime of this material, together with its non-absorbency of water are the main features. The spheres had an approximate wall thickness of 0.3 mm and served solely as non-structural void formers within the slab system. 100 or 144 balls are used for each specimen depending on the configuration.

The PVC spheres were placed between the upper and lower reinforcement meshes and were restrained by the reinforcement cage. In addition, the bottom reinforcement mesh was tied to the timber formwork using steel wires to prevent flotation or displacement of the spheres during concrete casting.

2.2. Specimen Parameters

Twelve specimens were manufactured with 2000 mm in longitudinal and transverse dimensions and 200 mm in section depth. The specimen parameters are summarized in Table 3. The design was based on reinforcement types:

- Slabs reinforced with GFRP (9 specimens).
- Three specimens of conventional steel-reinforced slabs.
- Two essential geometric patterns are derived from:
- Ribbed slab (three specimens - control)
- Bubble Deck slab (nine specimens)

In addition, there are three specimens with diaphragm reinforcement and nine specimens without diaphragm reinforcement. Void formers were distributed in different grid configurations, shown in Figures (1) and (2), The concrete volume reduction was dependent on the void configuration. The employment of 100 spherical voids led to volume reductions of about 5.4% and 12.8% for diameters of 94 mm and 125 mm, respectively, while increasing the number of 125 mm voids to 144 spheres increased the reduction ratio to approximately 18.5%. Although BubbleDeck systems reported in the literature can achieve concrete volume reductions of approximately 30–35%, the reduction obtained in the present study was limited to about 18.5%. This difference is mainly attributed to the presence of solid diaphragm regions at the loading zone and solid edge zones required for specimen fabrication and testing. These solid regions reduced the overall volume occupied by the spherical voids and consequently lowered the achievable concrete volume reduction compared with full-scale commercial BubbleDeck systems. The slab specimens were intentionally configured as under-reinforced sections to ensure that failure was governed either by rupture of the tension reinforcement or by compressive crushing of concrete subsequent to reinforcement failure. Figure 3. Specimen preparation process, including reinforcement placement, installation of PVC void formers, and concrete casting.

The clear concrete cover was maintained at 20 mm for all specimens. Accordingly, the effective depth of the slabs was approximately 175 mm for specimens reinforced with Ø10 bars and 172 mm for specimens reinforced with Ø16 bars. The diaphragm (DI) reinforcement arrangement consisted of five Ø16 mm bars distributed in each direction across the slab width. This reinforcement layout

was intended to provide a more uniform stress distribution and improve the structural performance of the slab under concentrated loading.

Table 3. Specimen Parameters

No.	Specimen ID	Rein.	Slab type	Loading	Void diameter (mm)	(D/H)*	Bottom Rein. Layout (mm)	Bottom Reinf. Area (As) (mm^2)	Section (Figure 2)
1	1R-S-M (Reference)	Steel	Ribbed	Monotonic	---	---	1-Φ16/ Rib	1005 (each direction)	A-A
2	1R-G-M	GFRP	Ribbed	Monotonic	---	---	1-Φ16/ Rib	1005 (each direction)	A-A
3	1R-G-RE	GFRP	Ribbed	Repeated	---	---	1-Φ16/ Rib	1005 (each direction)	A-A
4	1R-S-D125-M	Steel	BDS	Monotonic	125	0.625	1-Φ16/ Rib	1005 (each direction)	B-B
5	1R-G-D125-M	GFRP	BDS	Monotonic	125	0.625	1-Φ16/ Rib	1005 (each direction)	B-B
6	1R-G-D125-RE	GFRP	BDS	Repeated	125	0.625	1-Φ16/ Rib	1005	B-B
7	0.5R-G-D125-M	GFRP	BDS	Monotonic	125	0.625	Φ10@185+1-16	986 (each direction)	C-C
8	0R-DI-S-D125-M	Steel	BDS	Monotonic	125	0.625	5-Φ16	1005 (each direction)	D-D
9	0R-DI-G-D125-M	GFRP	BDS	Monotonic	125	0.625	5-Φ16	1005 (each direction)	D-D
10	0R-DI-G-D125-RE	GFRP	BDS	Repeated	125	0.625	5-Φ16	1005 (each direction)	D-D
11	0R-G-D125-M	GFRP	BDS	Monotonic	125	0625	Φ10@185	864 (each direction)	E-E
12	0R-G-D94-M	GFRP	BDS	Monotonic	94	0.47	Φ10@185	864 (each direction)	F-F

*Note: 1R=full ribbed slab; 0.5R=single central rib; 0R=slab without concrete ribs; DI=diaphragm reinforcement arrangement; S=steel reinforcement; G=GFRP reinforcement; M=monotonic loading; RE=repeated loading; D125 and D94=void diameter (mm), and BDS: BubbleDesck Slab. *: D: void diameter and H: the total slab thickness.*

Fig. 1. 3D Layout of the geometric specimens

.

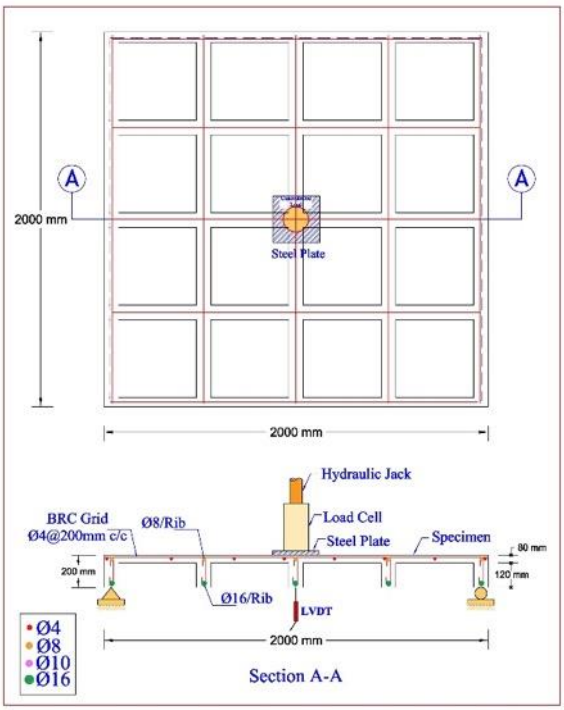

(a) (1R-S-M, 1R-G-M, and 1R-G-RE) specimens

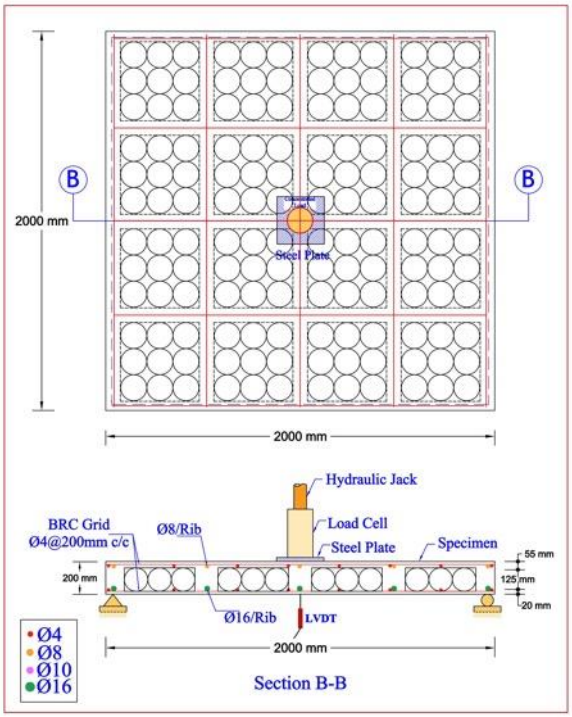

((b) (1R-S-D125-M, 1R-G-D125-M, and 1R-G-D125-RE) specimens

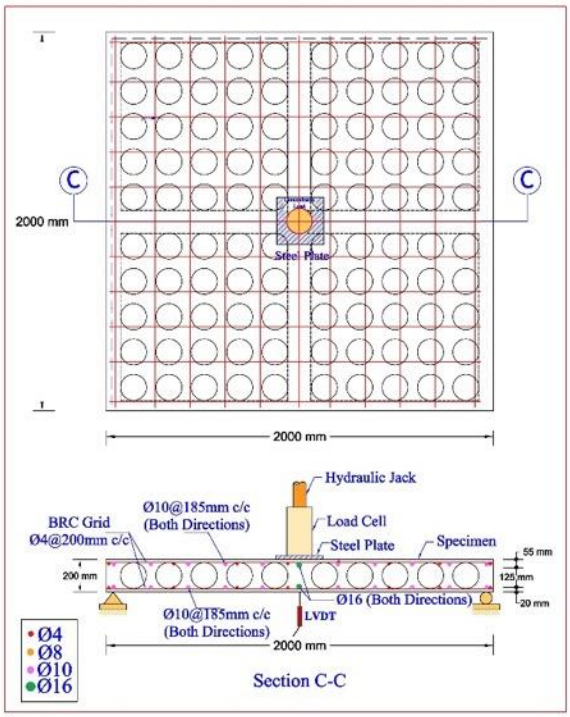

(c) (0.5R-G-D125-M) specimens

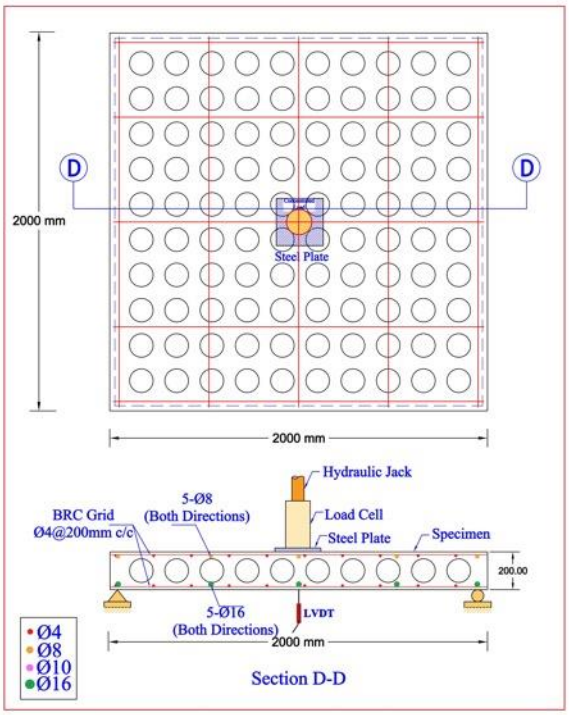

(d) (0R-DI-S-D125-M, 0R-DI-G-D125-M, and 0R-DI-G-D125-RE) specimens

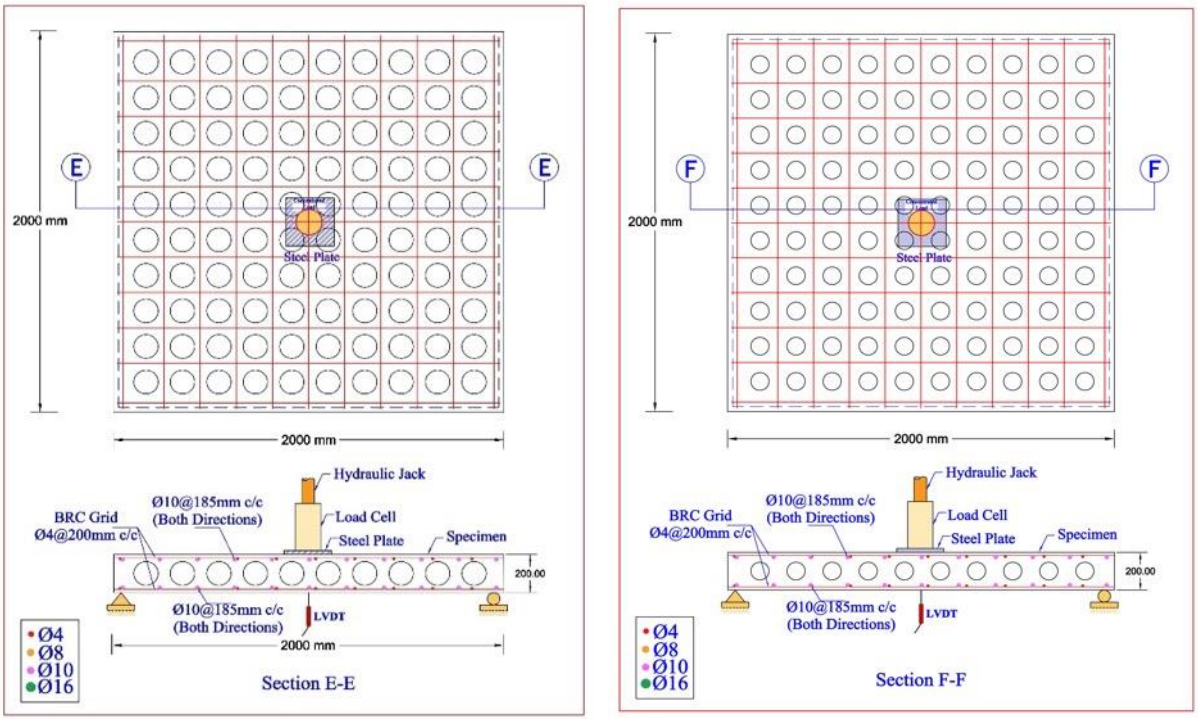

(e) (0R-G-D125-M) specimens (f) (0R-G-D94-M) specimens

Fig. 2. Geometric layout and reinforcement arrangement for the specimens

2.3 Experimental Setup

All specimens were subjected to testing using a hydraulic loading system. The slabs were supported on four edges by means of steel angle supports located 100 mm from each slab edge, resulting in an effective span of 1800 mm in both directions, simulating simply supported boundary conditions.

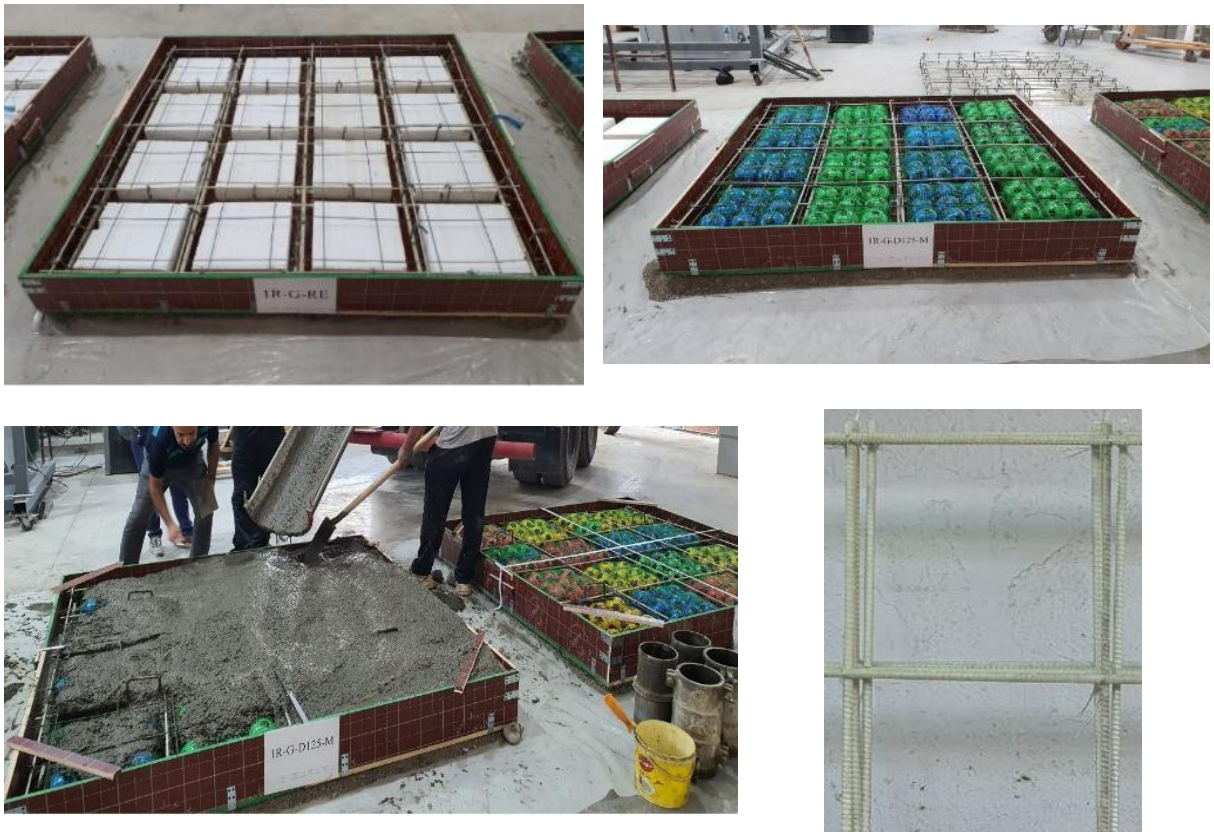

Fig. 3. Specimen preparation process

A central point load was applied through a steel loading plate with 250×250×250 mm section as shown in Figure (4). Instrumentation included [23]:

- Linear Variable Differential Transformer (LVDT): To measure deflection, a single LVDT was installed at the center of the slab directly beneath the loading point and was placed in contact with the bottom concrete surface to record the maximum mid-span deflection, as shown in Figure (5).
- Strain Gauges: An electric resistance strain gauge was bonded to the main tensile reinforcement of all specimens (steel and GFRP bars) at the position which is expected to undergo the maximum bending moment at midspan of the clear span. In this way, the measured strains represent the most critical bending state. Before and after casting the strain gauge was tested for accuracy and to remove thermal variation effects.
- Load Cell: installed directly on the hydraulic actuator with a maximum capacity of 100 Tons to provide accurate measurement of the applied load.

Fig. 4. Experimental test setup

Fig. 5. Test progress

2.4. Loading Protocol

2.4.1. Monotonic loading

Nine specimens were subjected to monotonic loading until failure. The load was applied in a single direction under load-controlled conditions at a constant rate of 0.5 kN/s using a hydraulic actuator.

2.4.2. Repeated Loading

The series of repeated loads was conducted in a load-controlled mode, by applying a unidirectional load from zero up to a predefined peak load followed by unloading to residual level, without the load being reversed. This procedure was intended to simulate sustained or extended live gravity loading, similar to running machinery or mild vehicular traffic [30,31]. Decrease of stiffness and

hysteretic dissipation of energy were investigated by a sequence of incremental increasing load cycles [23]:

- Load Increments and Cycles: Specimens 1R-G-RE and 0R-DI-G-D125-RE were subjected to repeated loads with an increment of 5 kN. On the contrary, for specimen 1R-G-D125-RE, a greater increment of 10 kN was used to minimize the total number of loading cycles while ensuring an appropriate resolution of the load-deflection response. Loading increments were set according to the estimated stiffness and load carrying capacity of the specimens under test as shown in Figs. (6) and (7). A full loading-unloading cycle was performed at the end of each increment before proceeding to the following load increment.
- Loading Cycle: All cycles were conducted quasi-statically to eliminate dynamic inertial effects and to make sure that the measured deflection accurately reflects material degradation/bond behavior, All loading cycles were conducted under load-controlled conditions at a rate of 0.5 kN/s.
- Failure Criterion: The test was terminated when a significant loss of load-carrying capacity occurred, excessive deformation developed, or a clear failure mechanism was observed. The number of cycles sustained by each specimen prior to failure is presented and discussed in the section 3.3.

This rigorous approach guarantees that the measured drops of stiffness and energy dissipation are properly characterized under the applied test conditions.

3. Experimental Results and Discussion

The test program studied the full-scale behavior of ribbed and voided (BubbleDeck) slabs with steel and GFRP bars under monotonic (M) and repeated (RE) loading conditions. The results highlighted the effects of reinforcement type, slab configuration (ribbed vs voided slab), and loading regime on key response parameters, including ultimate load capacity, load-deflection behavior, and peak reinforcement strain, as presented in Table 4 and illustrated in Figures 8-10.

Table 4. Specimens' experimental results

No.	Specimen ID	Load at crack stage, P_{cr} (kN)	Ultimate load, P_u (kN)	Reduction in ultimate load compared to control (%)	Deflection at ultimate load, Δ_u (mm)	Max. deflection, Δ_m (mm)	Max. Midspan Steel Strain, ε_u ($\times 10^{-6}$)
1	1R-S-M	57.2	224.202	0.0	12.65	13.38	6790
2	1R-G-M	16.9	120.357	-46.3%	52.45	58.69	2282
3	1R-G-RE	22.9	146.028	-34.9%	33.92	41.5	3954
4	1R-S-D125-M	31.1	154.542	-31.1%	21.06	30.11	4771
5	1R- G-D125-M	21.2	121.389	-45.9%	34.03	43.45	1041
6	1R-G-D125-RE	25.2	112.746	-49.7%	49.67	68.69	7823
7	0.5R-G-D125-M	48.5	180.084	-19.7%	33.61	42.31	5543
8	0R-DI-S-D125-M	41.5	237.747	+6.0%	23.96	27.3	5852
9	0R-DI-G-D125-M	34.1	147.358	-34.3%	30.5	34.9	3250
10	0R-DI-G-D125-RE	23.9	118.551	-47.1%	34.14	48.09	2730
11	0R-G-D125-M	43.2	183.051	-18.4%	24.84	28.45	8228
12	0R-G-D94-M	39.6	167.442	-25.3%	34.83	38.8	4134

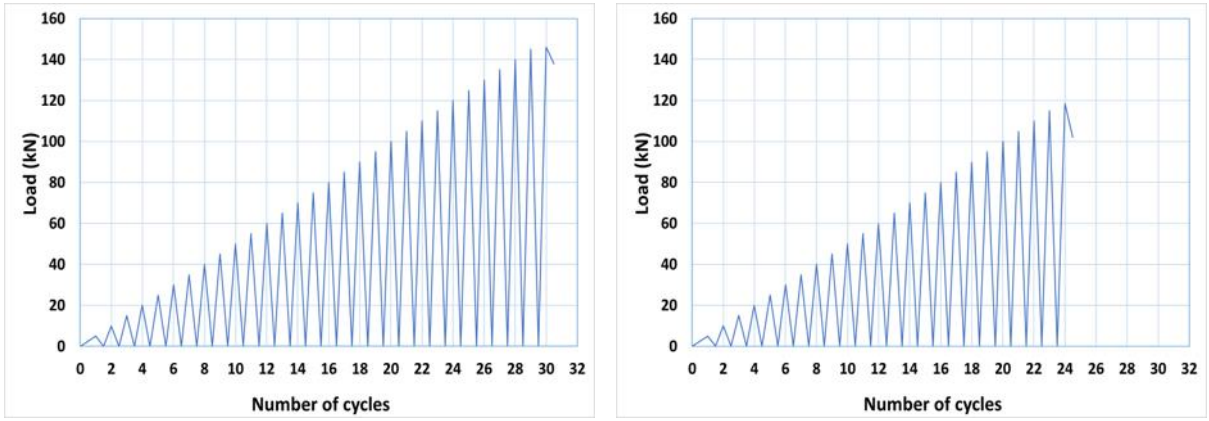

(a) 1R-G-RE (b) 0R-DI-G-D125-RE

Fig. 6. Repeated loads pattern of specimens (1R-G-RE and 0R-DI-G-D125-RE)

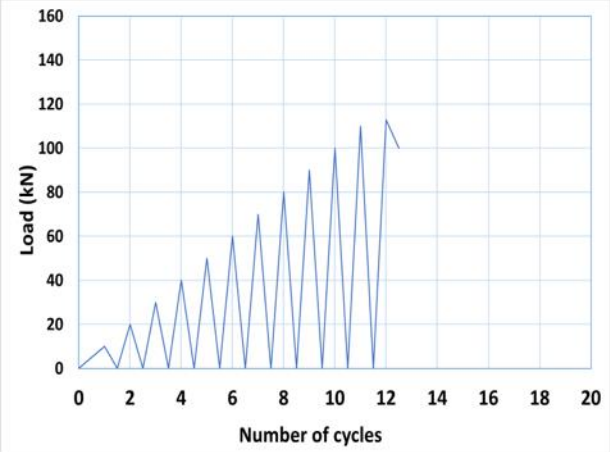

Fig. 7. Repeated loads pattern of specimen (1R-G-D125-RE)

3.1 Crack Initiation and Propagation

Crack development in all tested slabs followed a typical sequence for two-way reinforced concrete slabs subjected to central concentrated loading. Initial cracking occurred at the slab center beneath the loading plate where the maximum bending moment developed. As the load increased, cracks propagated radially toward the slab edges forming a star-shaped pattern typical of two-way slab systems. The initial cracking load for the control ribbed slab (1R-S-M) was recorded as 57.2 kN (Table 4), representing the highest value among all tested specimens. In contrast, the GFRP-reinforced ribbed slab 1R-G-M exhibited its first crack at 16.9 kN, which is approximately 70% lower than the steel-reinforced specimen. This variation can be explained by the higher modulus of elasticity of steel reinforcement, which delays crack formation by increasing the flexural stiffness of the slab.

Voided slab (BubbleDeck slabs) showed cracking loads varying between 21.2 kN and 48.5 kN. Specimen 0.5R-G-D125-M recorded the highest cracking load among the BubbleDeck specimens (48.5 kN), The relatively high cracking load of specimen 0.5R-G-D125-M can be attributed to the presence of the central concrete rib combined with concentrated reinforcement beneath the loading region. This configuration increased the local stiffness and improved stress transfer within the critical zone subjected to maximum tensile stresses. Consequently, crack initiation was delayed and stress concentrations around the spherical voids were reduced compared with the other BubbleDeck configurations.

Crack propagation was strongly influenced by reinforcement type. Steel-reinforced slabs generally developed fewer but wider cracks, whereas GFRP-reinforced slabs developed a larger number of closely spaced cracks due to the lower stiffness of the reinforcement. In addition, the crack growth

in GFRP-reinforced slabs was affected by the bond at the GFRP–concrete interface. Localized bond-slip and progressive debonding may have led to the formation of a higher number of closely spaced cracks with a lower post cracking stiffness in these specimens. In addition, the crack patterns in the BubbleDeck slabs were affected by the presence of spherical voids. The cracks tended to propagate along the concrete ribs located between adjacent voids, indicating that these ribs acted as the primary load-transfer paths and governed the crack propagation mechanism within the slab system. For specimens subjected to repeated loading, crack growth showed a pattern of cumulative increase during the cycles of loading. Existing cracks tended to reopen and propagate further during reloading, while partial crack closure occurred during unloading stages. This repeated opening and closing mechanism accelerated stiffness degradation and promoted wider crack propagation compared with the monotonic loading specimens. The lower modulus of elasticity and bond slip at the interface between reinforcement and concrete in the slab subjected were the cause of more pronounced crack development and higher residual strain in the GFRP-reinforced slabs under repeated loading.

3.2 Load-Deflection Behavior

Figure (8) presents the load-deflection responses under monotonic loading conditions. The control ribbed slab 1R-S-M shows the steepest initial slope, indicating the highest stiffness. This specimen attained an ultimate load of 224.2 kN, accompanied by a corresponding deflection of 12.65 mm. While the ribbed slab with GFRP reinforced (1R-G-M) reached an ultimate load of 120.36 kN, which represents a 46.3% reduction compared with the reference specimen (1R-S-M) as illustrated in Figure (8). Nevertheless, the maximum deflection increased significantly to 58.69 mm, demonstrating the lower stiffness and higher deformability of samples with GFRP reinforcement. Although the GFRP-reinforced specimen carried sufficient load-carrying capability, the much greater deflection indicates the importance of serviceability aspects in GFRP design. Therefore, due consideration should be given to the deflection control requirements of ACI 440.1R [32] in the design of GFRP-reinforced slab systems.

In general, BubbleDeck slabs exhibited lower stiffness than the ribbed control slab attributed to the presence of spherical voids, which reduce the effective volume of concrete. Specimen 1R-S-D125-M reached an ultimate load of 154.54 kN, corresponding to a 31.1% reduction relative to the control specimen. However, some BubbleDeck configurations demonstrated good performance. Specimen 0R-DI-S-D125-M achieved the highest ultimate load of 237.75 kN, exceeding the control slab by approximately 6%, which highlights the beneficial role of diaphragm reinforcement in improving load transfer and structural integrity. The improved structural response can be attributed to the additional diaphragm reinforcement, which enhanced force distribution and stress transfer within the slab system. The increased reinforcement concentration in the diaphragm region contributed to delaying crack propagation and improving the overall load-carrying mechanism.

Steel reinforced slabs showed a visible yielding plateau in the load-deflection response, indicating a ductile behavior and progressive energy dissipation after steel yielding. The GFRP reinforced slabs, on the other hand, showed an almost linear-elastic behavior up to failure without a distinguishable yielding stage, due to the brittle character and lower elastic modulus of the GFRP bars. The more significant deflections in the GFRP specimens were predominantly due to a reduction in post-cracking stiffness rather than material ductility.

3.3 Effect of Repeated Loading

Specimen 1R-G-RE sustained 30 loading cycles, and specimen 0R-DI-G-D125-RE survived for a total of 24 cycles before ultimate capacity failure. The total number of cycles for the 1R-G-D125-RE sample is 12. The load-deflection characteristics for the specimens under repeated loading are depicted in Figure (9). Detailed inspection of these curves indicates that the structural responses for 1R-G-RE, 1R-G-D125-RE, and 0R-DI-G-D125-RE closely mirror the phases identified in monotonic tests, albeit with a progressive degradation in stiffness. During the primary loading cycle, the behavior within the crack-opening regime remains comparable with the pre-cracking and incipient post-cracking intervals observed in static benchmarks. This initial damage induces a

perceptible decline in the section's initial stiffness (Ki) before subsequent damage cycles accumulate.

Secondly, the unloading and reloading (Hysteretic Energy) path is a curved line within the closed loop load path as opposed to a straight-line path in open path load cycles. The energy dissipated by hysteresis can be calculated from the loop area. This energy is the added internal (from internal friction), and external energy associated with crack growth and material damage or strain (from fracture propagation and material strain), i.e. it is the total energy required per unit volume of material to locally fracture. The hysteretic behavior observed under repeated loading was consistent with the toughness presented in Table 5. Among the tested specimens, 1R-G-D125-RE exhibited the highest total toughness (6061.1 kN·mm), indicating superior energy dissipation capacity under repeated loading conditions.

Consequently, the stiffness degradation leads to a varying strain reloading curve in each cycle. The decrease in secant stiffness reveals debonding and crack propagation at the GFRP concrete interface. The presence of residual deflection indicates that the unloading curve intersects the X-axis at a positive deflection ($\Delta_{residual}$) above the origin. The $\Delta_{residual}$ is the accumulated deformation (due to the accumulation of plastic strain) induced when bonds shift and micro-damage occurs.

Repeated loading produced noticeable load-deflection hysteresis loops, indicating progressive stiffness degradation and evolution of energy dissipation capacity across the successive loading cycles.

Specimen 1R-G-RE reached an ultimate load of 146.03 kN, which is higher than the monotonic specimen 1R-G-M (120.36 kN). Although the repeated loading usually causes the loss of stiffness and accumulation of damage, the 1R-G-RE specimen showed a higher ultimate load than the monotonic one. This pattern can be explained by progressive stress redistribution and cracks stabilization in the early cycles of loading, which delayed the development of critical localized cracking below the loading zone. Another possible explanation could be that localized bond-slip or partial debonding between GFRP bars and surrounding concrete could have happened sooner in the monotonic specimen, which caused premature stress concentration and worse load-transfer efficiency. However, the repeatedly loaded specimens still exhibited higher deflections, bigger cracks and apparent stiffness loss before failure.

3.4 Effect of Reinforcement Type (Steel vs GFRP)

A study was carried out to investigate the effect of the reinforcing material's stiffness on structural behavior, contrasting specimens reinforced with steel with those reinforced with GFRP bars.

Considering slabs with ribs, a steel specimen (1R-S-M) has an ultimate load of 224.2 kN. The ultimate load applied to the GFRP specimen (1R-G-M) was 120.36 kN. The ultimate load capacity of the specimens with steel reinforced was 86% greater than that of the GFRP-reinforced slab as shown in Figure (10). A similar trend regarding the influence of reinforcement type was observed in BubbleDeck slabs. Unlike specimen 1R-G-D125-M, which attained an ultimate load capacity of 121.39 kN, specimen 1R-S-D125-M sustained a higher ultimate load of 154.54 kN. In this instance, the incorporation of steel reinforcement enhanced load capacity by around 27 percent.

The effect of reinforcing type was more significant in the ribbed slabs, where the structural behavior was mainly dominated by flexural action. On the other hand, the voids in the BubbleDeck slabs influenced the stress transmission mechanism and increased the contribution of the concrete ribs and slab geometry, thus decreasing the relative effect of the reinforcement type on the ultimate load capacity. The GFRP-reinforced slabs exhibited markedly greater deflections, indicating enhanced deformability. This phenomenon occurs notwithstanding the decrease in the load-carrying capacity of the slabs. The maximum deflection of specimen 1R-G-M was 58.69 mm, almost 4.4 times larger than that of the control slab reinforced with steel. The deflection of the GFRP-reinforced slab is much higher than that of the steel-reinforced slab, mainly due to the lower elastic modulus of GFRP bars in comparison to steel reinforcement. The elastic modulus of the steel reinforcement (200 GPa) is nearly four times that of the GFRP bars (~50 GPa) as seen clearly in Table 2. The considerable differential in stiffness caused the GFRP-reinforced slab to have a lower

flexural rigidity after cracking and resulted in much higher deflections under similar loading circumstances.

3.5 Effect of BubbleDeck Voids

The introduction of spherical plastic voids reduces the self-weight of the slab by eliminating concrete from regions of low stress. However, this modification also influences structural stiffness and strength. Comparing the results of the ribbed slab (1R-S-M) with the BubbleDeck slab 1R-S-D125-M shows that the presence of voids reduced the ultimate load from 224.2 kN to 154.54 kN, corresponding to a 31% reduction.

Although the introduction of voids resulted in a reduction in ultimate load capacity, the BubbleDeck system still provided a favorable balance between structural performance and material savings through the reduction of concrete volume and self-weight. The concrete ribs between the voids effectively carried the flexural stresses, allowing the slab to maintain adequate load capacity. The concrete ribs between adjacent voids acted as the primary load-transfer paths, carrying flexural stresses and maintaining structural continuity across the slab despite the reduction in concrete volume.

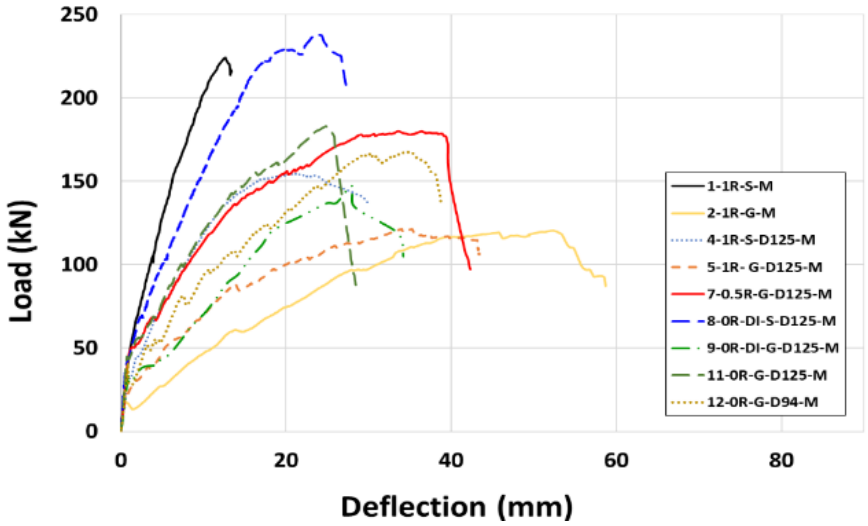

Fig. 8. The relationship between the applied load and the resulting mid-span deflection for specimens under monotonic loading

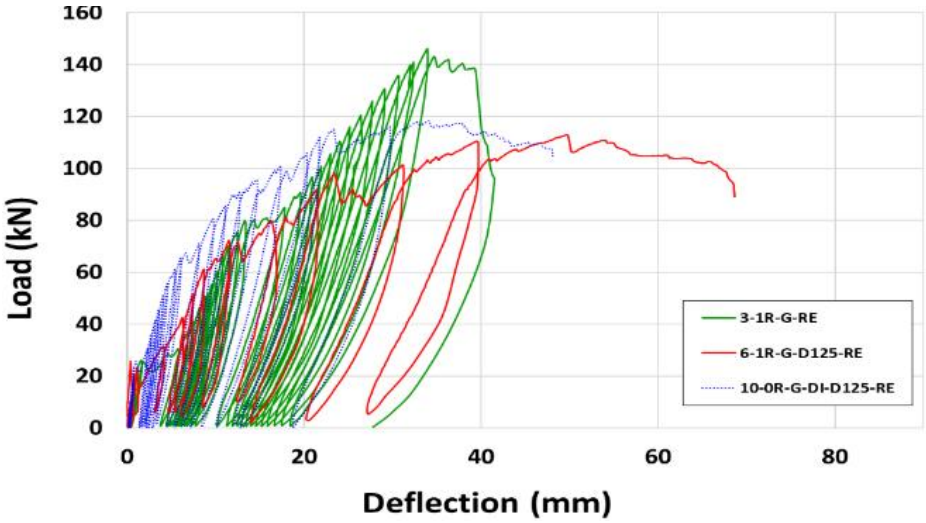

Fig. 9. The relationship between the applied load and the resulting mid-span deflection for specimens under repeated loading

Additionally, specimen 0R-G-D94-M, which used 94 mm voids, achieved an ultimate load of 167.44 kN, the reduction of the void diameter from 125 mm to 94 mm did not increase the ultimate load capacity. The sample with 125 mm voids (0R-G-D125-M) displayed higher ultimate load than its direct equivalent with 94 mm spaces (0R-G-D94-M). However, the specimen with smaller voids showed better deformability and energy absorption characteristics which can be due to the existence of more continuous concrete matrix between voids.

Table 5. Summary of stiffness and energy absorption properties of the specimens

No.	Specimen ID	Initial Stiffness, K_i (kN/mm)	Post-Cracking Stiffness, K_{pc} (kN/mm)	Stiffness Retention (%)	Energy Absorption (Toughness)			Deformability Index
					Pre-Cracking, U_{pre} (kN.mm)	Post-Cracking, U_{post} (kN.mm)	Total Toughness U_{Total} (kN.mm)	
1	1R-S-M	39.72	14.90	37.5	48.40	1897.4	1945.80	-
2	1R-G-M	19.88	2.00	10.1	6.50	4970.1	4976.60	6.03
3	1R-G-RE	19.08	3.76	19.7	15.40	3565.5	3580.90	3.73
4	1R-S-D125-	35.75	6.11	17.1	13.80	3631.5	3645.30	-
5	1R- G-	40.77	2.99	7.3	6.50	3963.3	3969.80	8.51
6	1R-G-D125-	63.00	1.78	2.8	13.50	6047.6	6061.10	8.42
7	0.5R-G-	44.09	4.05	9.2	29.40	5819.9	5849.30	10.84
8	0R-DI-S-	56.85	8.45	14.9	17.70	4639.4	4657.10	-
9	0R-DI-G-	35.15	3.84	10.9	17.20	3284.3	3301.50	5.26
10	0R-DI-G-	31.87	2.83	8.9	8.40	4581.3	4589.70	10.91
11	0R-G-D125-	63.53	5.79	9.1	13.70	3580.1	3593.80	7.31
12	0R-G-D94-	48.89	3.76	7.7	14.70	4614.4	4629.10	6.52

3.6 Effect of Diaphragm Reinforcement

Diaphragm reinforcement was introduced to improve load distribution between the slab ribs. It is possible to clearly highlight this impact by comparing specimens that have and do not have diaphragm reinforcement. The steel reinforcement ultimate capacity is 154.54 kN for 1R-S-D125-M, and 237.75 kN for 0R-DI-S-D125-M.

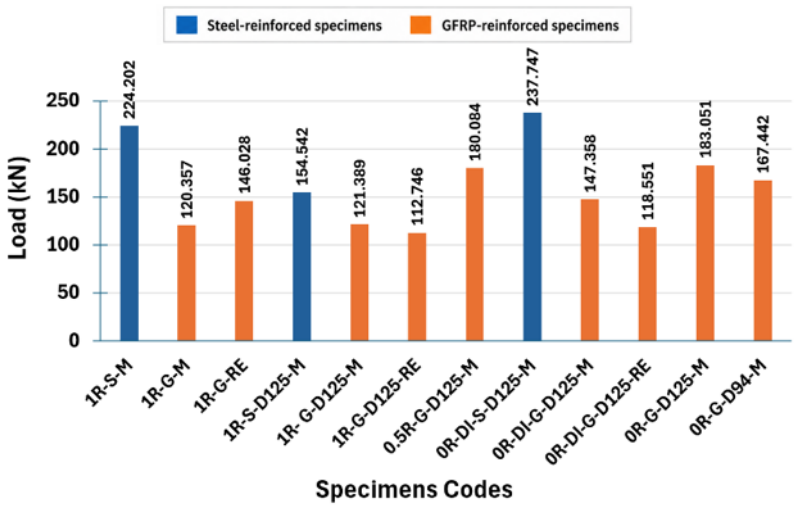

Fig. 10. Ultimate load of specimens

An increase of about 54% in load capacity was obtained by the use of diaphragm reinforcement. The comparison between specimen 0R-G-D125-M and specimen 0R-DI-G-D125-M for the GFRP reinforced specimens revealed that the diaphragm reinforcement configuration did not increase

the ultimate load capacity. But diaphragm configuration helped in better cracking distribution, improved stress redistribution and greater structural stability at loading stages.

3.7 Crack Pattern

All tested slabs showed cracking patterns typical of two-way reinforced concrete slabs under a central concentrated load. The first cracks appeared at the slab center beneath the loading plate and then propagated radially toward the edges as the load increased.With further loading, additional cracks formed and intersected with the radial cracks, producing a network of orthogonal and diagonal cracks that gradually developed into a distinct yield-line pattern. This crack pattern is typical for two-way slabs under concentrated load and corresponds to the development of plastic lines of hinges in the slab. These hinge lines, as the loading increased, took on the shape of rigid slab portions rotating about each other, resulting in a collapse mechanism having the form postulated in the classical yield-line theory for RC slabs. In BubbleDeck slabs, the spherical plastic voids had a major impact on crack behavior. The alternation of solid concrete ribs and void spaces also affected the stress field inside the material and produced larger crack openings and fewer cracks than in typical ribbed slabs. The concrete ribs between the voids took the majority of the loads, and cracks typically propagated along these ribs where tensile stresses were focused. The failure mode of the tested slabs can be divided into three major categories based on the test results as shown in Figure (11): (a) Localized flexural failure, (b) Distributed yield-line flexural, and (c) Flexural-punching interaction failure. So, localized flexural failure refers to specimens in which failure was dominated by concentrated flexural cracking near the loading zone without the formation of a fully distributed yield-line mechanism across the slab surface. In contrast, distributed yield-line flexural failure describes specimens that developed extensive crack networks and multiple yield-line patterns prior to failure, indicating broader moment redistribution within the slab system.

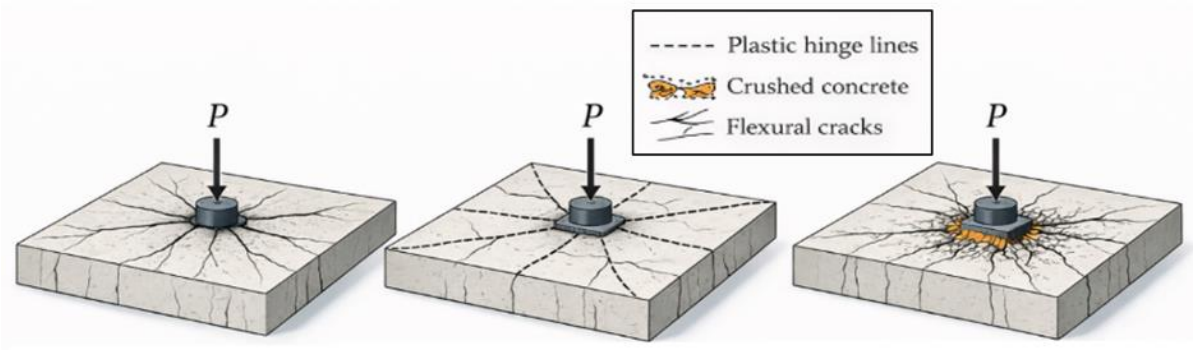

(a) (b) (c)

Fig. 11. Failure mechanisms of specimens (a) localized flexural failure, (b) distributed yield-line flexural failure, and (c) flexural-punching interaction failure

The majority of specimens exhibited flexural yield-line failure, which is typical for two-way slab systems subjected to concentrated loading. In these cases, radial cracks emanated from the loading point and extended toward the slab edges, eventually forming a well-defined yield-line mechanism. Several specimens, namely Specimens 2, 4, 7, and 11, showed a mixed flexural-punching interaction mode of failure. In these slabs localized crushing and concrete damage occurs under the loading plate, together with the flexural cracking pattern. This bending and punching shear interaction was due to the magnification of the stresses near the loading zone and the presence of voids that reduce the cross-section of concrete around these voids. It should be noted that a solid concrete region was provided beneath the loading area. Although the dimensions of the loading plate exceeded those of the solid region, the central portion of the load was transferred through solid concrete. Consequently, the spherical voids were not located directly beneath the center of loading, although they may have influenced the surrounding stress distribution and the overall punching shear behavior. The complete failure categories are presented in Tables (6) and Figures (12) and (13) for pictorial description. However, Specimens 1 and 3 failed in localized flexural

manner since the rebar attained its tensile capacity without punching damage being significant. Extensive flexural cracking and large deflections controlled the failure, with ultimate collapse following. Overall, the experimental observations indicate that the structural behavior of BubbleDeck slabs remains predominantly governed by flexural mechanisms similar to those observed in conventional two-way reinforced concrete slabs. Despite the presence of internal voids, the load transfer was effectively carried through the concrete ribs between the spheres, allowing the slabs to develop classical yield-line failure patterns.

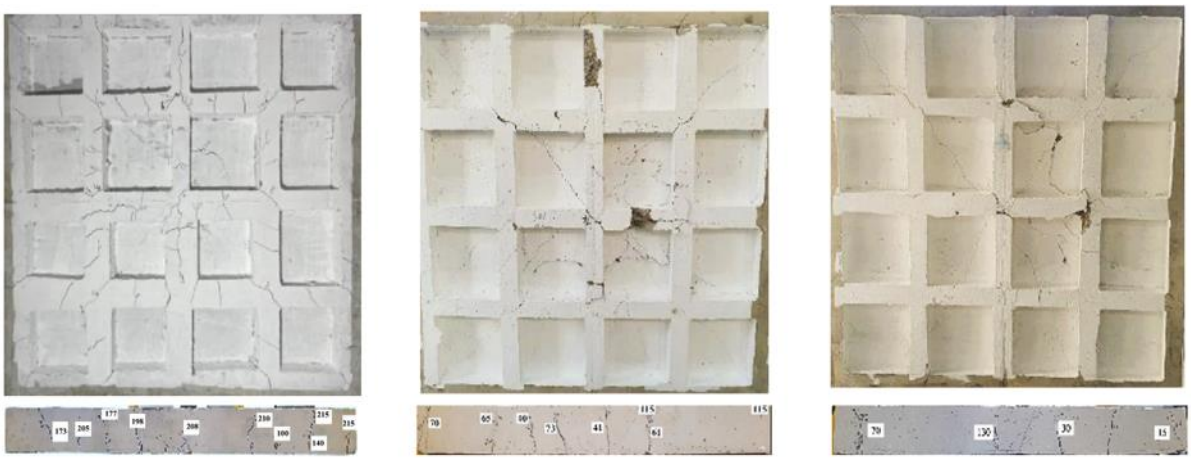

1-1R-S-M 2-1R-G-M 3-1R-G-RE

Fig. 12. Failure modes and crack patterns of ribbed slab specimens at the ultimate stage

Table 6. Failure mode of specimens

No.	Specimen code	Failure Mode
1	1R-S-M	Localized flexural
2	1R-G-M	Flexural-punching interaction
3	1R-G-RE	Localized flexural
4	1R-S-D125-M	Flexural-punching interaction
5	1R- G-D125-M	Distributed yield-line flexural
6	1R-G-D125-RE	Distributed yield-line flexural
7	0.5R-G-D125-M	Flexural-punching interaction
8	0R-DI-S-D125-M	Distributed yield-line flexural
9	0R-DI-G-D125-M	Distributed yield-line flexural
10	0R-DI-G-D125-RE	Distributed yield-line flexural
11	0R-G-D125-M	Flexural-punching interaction

Table (7) listed the values of crack width at service stage ($W_{Service}$), ultimate crack width ($W_{Ultimate}$), and the cracks spacing at ultimate load stage ($S_{Ultimate}$), based on the following aspects:

- Maximum Service Load Crack Width ($W_{Service}$): In the case of all specimens, the maximum crack width occurred at the normal service load ($P_{Service}$= 0.4 $P_{Ultimate}$). The results show that the maximum crack width of all GFRP specimens was kept below the ACI 440.1R limit of 0.70 mm for interior exposure environment.
- Ultimate Failure Crack Width ($W_{Ultimate}$): Maximum crack width at ultimate, approximately 7.8 mm. The large crack opening is mainly due to the low elastic modulus and large deformability of the GFRP reinforcement, which causes larger crack development before failure. The measured crack width is the last step of loading when large crack growth has already been reached and concrete crushing in the compression zone happened. Therefore, the significant fracture width does not necessarily mean that the GFRP bars have ruptured, but it instead indicates the advanced flexural damage and ultimate failure condition of the specimen.

- Experimental Crack Spacing, the measured ultimate crack spacing ($S_{Ultimate}$) expresses how well the tensile strain is spread by the reinforcing arrangement.

Table 7. Specimens' cracks width and spacing characteristics

No.	Specimen ID	Pu, exp (kN)	Max. strain,exp ($\times 10^{-6}$)	Calculated $f_{Ultimate}$* (MPa)	$W_{service}$** (mm)	$W_{service}/W_{limit}$	$W_{Ultimate}$ (mm)	$S_{Ultimate}$ (mm)
1	1R-S-M	224.202	6790	1358.0	0.120	0.30	1.95	135
2	1R-G-M	120.357	2282	114.1	0.169	0.24	3.8	210
3	1R-G-RE	146.028	3954	197.7	0.046	0.07	4.5	185
4	1R-S-D125-M	154.542	4771	954.2	0.090	0.23	3.1	250
5	1R- G-D125-M	121.389	1041	52.05	0.0439	0.06	3.45	230
6	1R-G-D125-RE	112.746	7823	391.15	0.275	0.39	4.1	195
7	0.5R-G-D125-M	180.084	5543	277.15	0.0423	0.06	5.2	170
8	0R-DI-S-D125-M	237.747	5852	1170.4	0.060	0.15	4.85	180
9	0R-DI-G-D125-M	147.358	3250	162.5	0.082	0.12	5.3	195
10	0R-DI-G-D125-RE	118.551	2730	136.5	0.031	0.04	7.8	290
11	0R-G-D125-M	183.051	8228	436.084	0.110	0.16	5.4	205
12	0R-G-D94-M	167.442	4134	219.102	0.288	0.41	4.25	265

*: $f_{Ultimate} = E \times \in_{Max}$, *E_s=200 GPa uses in calculation of $f_{Ultimate}$ for steel specimens, while GFRP samples use E_f = 50 GPa.*

**: $W_{Service} = 2.\frac{f}{E}.\beta.K_b.\sqrt[2]{{d_c}^2.(\frac{s}{2})^2}$

4-1R-S-D125-M

5-1R-G-D125-M

6-1R-G-D125-RE

7-0.5R-G-D125-M

8-0R-S-D125-M

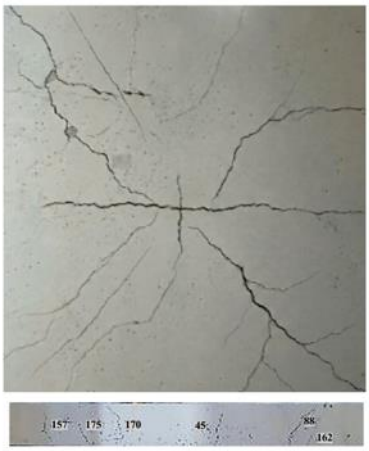

9-0R-G-D125-M

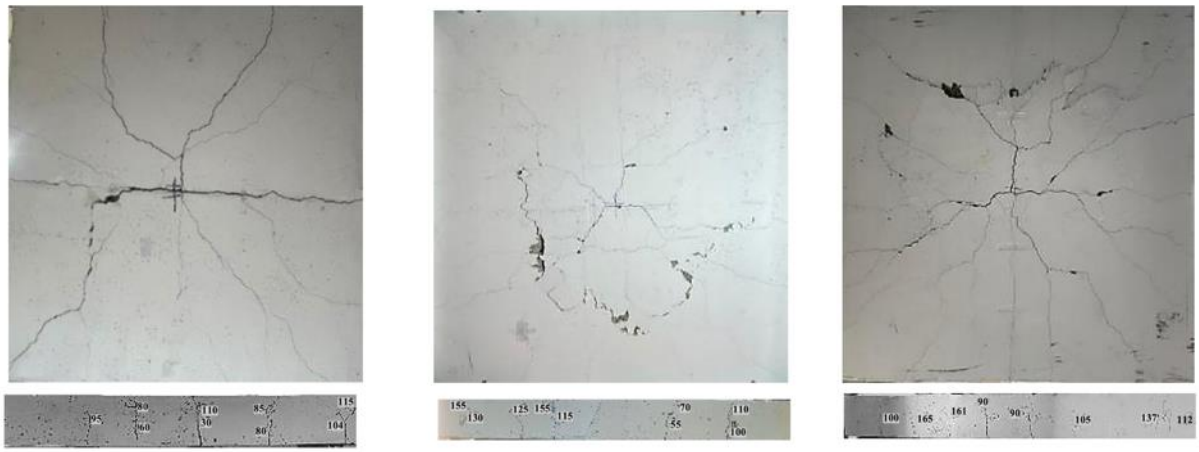

10-0R-DI-G-D125-RE 11-0R-G-D125-M 12-0R-G-D94-M

Fig. 13. Failure modes and crack patterns of voided slab specimens at the ultimate stage

- Serviceability: All tested specimens met the serviceability criteria. The predicted crack widths at service load remained below the recommended limits of 0.40 mm for steel-reinforced slabs and 0.70 mm for GFRP-reinforced slabs in accordance with ACI recommendations.
- Cracking behavior of GFRP specimens: The GFRP reinforced specimens, in particular specimen 0R-DI-G-D125-RE, showed extremely small, expected service crack width about 0.031 mm. For GFRP reinforcement wider cracks are assumed to be obtained at ultimate loads due to the low elastic modulus, however, the crack widths at service load (0.4Pu) were very small and under the limits allowed by the code.

3.8. Stiffness and Energy Absorption Capacity

3.8.1 Initial Stiffness and Deterioration

The stiffness and energy absorption capacity (toughness or hysteretic energy) of both GFRP- and steel-reinforced concrete slab specimens are presented in Table 5. The tested slabs were evaluated using initial stiffness (Ki), representing the slope of the load-deflection curve before cracking, and post-cracking stiffness (Kpc), which indicates the residual stiffness of the structure after crack development and internal stress redistribution. As shown in Table 5, the initial stiffness values ranged from 19.08 to 63.53 kN/mm, indicating a strong influence of reinforcement type and slab configuration. The initial stiffness for the steel-reinforced ribbed control slab (1R-S-M) was 39.72 kN/mm, and the GFRP-reinforced ribbed slab (1R-G-M) experienced a dramatic drop in stiffness down to 19.88 kN/mm, about 50% lower. This is because the modulus of elasticity of GFRP bars is less than that of the steel reinforcement. For the BubbleDeck slabs, the initial stiffness varied between 35.15 and 63.53 kN/mm, and a few of the samples showed stiffness that was comparable to or higher than that of the control slab. For instance, the specimen 0R-G-D125-M attained the maximum stiffness of 63.53 kN/mm which signifies that the concrete ribs separating the plastic spheres can withstand bending moments even with internal voids. Despite the elastic modulus of steel reinforcement is much higher than GFRP bars, the relatively high initial stiffness for specimen 0R-G-D125-M can be attributed to the more uniform reinforcement distribution and improved load-transfer mechanism along the slab surface at early uncracked loading stage. Therefore, the first obtained stiffness depends on the slab configuration, load distribution and uncracked concrete behavior and not only on the reinforcing stiffness.

The effect of diaphragm reinforcement arrangement on the initial stiffness was dependent on the reinforcement type. For the specimens with steel reinforcement, the diaphragm arrangement raised the initial stiffness from 35.75 kN/mm to 56.85 kN/mm. However, the initial stiffness of the GFRP reinforced specimens was reduced from 63.53 kN/mm for specimen 0R-G-D125-M to 35.15 kN/mm for specimen 0R-DI-G-D125-M. This result can be attributable to the interaction between the decreased elastic modulus of GFRP reinforcement and the modified stress-transfer mechanism

associated with the diaphragm reinforcement arrangement. Post-cracking, all specimens experienced a substantial decrease in stiffness. The control slab 1R-S-M showed the largest post-cracking stiffness (14.90 kN/mm), and although GFRP-reinforced specimens displayed lower results (for example, 2.00 kN/mm for 1R-G-M and 1.78 kN/mm for 1R-G-D125-RE). This reduction is the standard for GFRP reinforced members, because of their lower modulus elasticity and non-yielding behavior. Based on the results, it can be concluded that: i) the slab elasticity is mainly determined by the stiffness of the reinforcement; ii) BubbleDeck voids and the diaphragm reinforcement produce partial stress redistributions and consequently partial modification of the cracked behavior.

3.8.2 Energy Absorption Capacity (Total Toughness)

The capacity of the tested slabs for absorbing energy was calculated through the total toughness (U_{Total}) that is defined as the total area under the load-deflection curve to failure. This parameter indicates how much the slab can deform and absorb energy before collapse. For the GFRP-reinforced specimens, It should be noted that the high toughness values do not imply ductile material behavior of the reinforcement itself as steel reinforcement. Rather, the increased energy absorption capacity resulted from the large deflections and wider crack openings developed before failure. As can be seen from Table 5, the total toughness values are in the range of 1945.8-6061.1 kN·mm, which depends strongly on the reinforcement type of the slab, slab configuration and loading condition. The steel-reinforced ribbed control panel (1R-S-M) had the lowest toughness (1945.8 kN·mm) because of its small ultimate deflection (13.38 mm) although it has a high load capacity.

In contrast, the GFRP-reinforced ribbed slab (1R-G-M) demonstrated a much higher toughness of 4976.6 kN·mm, which is approximately 2.6 times greater than the control slab. This increase is mainly attributed to the larger deformation capacity of GFRP-reinforced slabs. For the BubbleDeck slabs, toughness values ranged from 3301.5 to 6061.1 kN·mm, generally exceeding that of the ribbed control slab. The highest toughness was recorded for 1R-G-D125-RE (6061.1 kN·mm), indicating that the combination of GFRP reinforcement and repeated loading significantly increased energy dissipation capacity. The enhanced toughness observed under repeated loading may be attributed to progressive micro-crack development and stress redistribution during the loading cycles, which increased the overall energy dissipation capacity prior to ultimate failure. Overall, the results indicate that GFRP reinforcement enhances the energy absorption capacity of slabs due to their greater deformation capability, while the presence of BubbleDeck voids does not significantly reduce the ability of the slab system to dissipate energy.

A comprehensive evaluation of slab performance requires the combined consideration of initial stiffness (Ki), ultimate load capacity (Pu), and energy absorption capacity (U_{Total}). These parameters as inputs are used to describe the bending, shear and combined responses of slabs. The control ribbed slab (1R-S-M) had a relatively high stiffness (Ki = 39.72 kN/mm) and was the highest loaded ribbed specimen with the maximum load of Pu = 224.2 kN. But due to its small deformation capacity, it was the least tough (U_{Total} = 1945.8 kN·mm). Unlike this, the GFRP-reinforced ribbed slab (1R-G-M) had a lower stiffness (Ki = 19.88 kN/mm) and a lower strength (Pu = 120.36 kN), but it had much higher energy absorption capacity (U_{Total} = 4976.6 kN·mm) due to larger deformations prior to failure.

For the BubbleDeck slabs, the voids did make a minor dent in the ultimate load capacity, but nothing major to the ductility. For instance, specimen 1R-G-D125-RE achieved the greatest toughness (U_{Total} = 6061.1 kN·mm) with a moderate ultimate load (Pu = 112.75 kN). Also, some BubbleDeck samples recorded high stiffness values such as 0R-G-D125-M (Ki = 63.53 kN/mm), proving that the concrete ribs between the voids do carry bending stresses efficiently. The pre-cracking and post-cracking toughness characteristics of steel- and GFRP-reinforced specimens were significantly different. The steel reinforced control slab (1R-S-M) showed much higher pre-cracking toughness because to the higher elastic modulus and stiffness of steel reinforcement which improved the resistance of crack initiation. In contrast, the GFRP-reinforced specimen (1R-G-M) demonstrated relatively small pre-cracking toughness but a much bigger post-cracking energy absorption. This behavior is mainly due to the lower elastic modulus of GFRP bars, which

reduced the post-cracking stiffness and permitted larger deflections and higher deformation capacity before failure.

Overall, the results indicate that steel reinforcement improves stiffness and strength, while GFRP reinforcement enhances deformation capacity and energy absorption. The effect of BubbleDeck voids on toughness was dependent on the type of reinforcement. The voided slabs displayed better toughness than the similar ribbed slab in the steel-reinforced specimens. This may be attributable to the ductile yielding behavior of the steel reinforcement, wider crack propagation and increased deformation capacity. On the other hand, the toughness of the GFRP-reinforced voided slabs was reduced compared to the corresponding ribbed slab due to the reduction in concrete volume and flexural stiffness.

3.9 Experimental Results Summary

The following key findings can be drawn from the experimental results:

- The steel-reinforced slabs were stiffer and stronger than the GFRP-reinforced ones. Whereas Steel reinforcement increased capacity by 86% relative to GFRP in ribbed slabs
- The deflections were larger in the GFRP-reinforced slabs, because of the smaller elastic modulus of the GFRP reinforcement.
- BubbleDeck slabs successfully reduced slab weight while maintaining acceptable structural performance. However, BubbleDeck reduced capacity by 31.1%.
- The effect of diaphragm reinforcement on structural performance was dependent on the type of reinforcement. The configuration of the diaphragm in the steel reinforced slabs raised the ultimate load capacity by 54%and improved the load distribution, Meanwhile, the GFRP-reinforced slabs did not show an increase in the ultimate load capacity due to the diaphragm arrangement, albeit the improvements in the stress redistribution and crack control behavior were noticed.
- Repeated loading resulted in stiffness degradation and increased energy absorption. So (1R-G-D125-RE) achieved the highest toughness of 6061.1 kN·mm. However, certain GFRP-reinforced specimens showed higher ultimate capacities than their monotonic counterparts, indicating the influence of stress redistribution and crack stabilization mechanisms and localized bond-slip reasons.
- Reducing the void diameter from 125 mm to 94 mm improved the deformability and energy absorption characteristics which can be due to the existence of more continuous concrete matrix between voids.

4. Numerical Simulation and Analysis of Design Variables

To further study the structural response of the test slabs, a nonlinear finite element model was developed using ABAQUS/CAE. The simulation model was established for the ribbed slabs and BubbleDeck slabs tested in the laboratory. The focus of the numerical analysis was to capture load-deflection relationship, crack pattern and rebar strain as measured during the tests program.

In this paper, concrete was simulated by using Concrete Damaged Plasticity (CDP) model, which is the commonly adopted model for modeling nonlinear response of reinforced concrete structures [21,22]. Table 8 summarizes the CDP parameters used in numerical simulations. This model allows the representation of concrete cracking under tension and crushing under compression through damage variables. The CDP model is capable of capturing stiffness degradation, crack propagation, and plastic deformation under repeated and monotonic loading conditions.

4.1 Finite Element Discretization

Three kinds of elements were used in the numerical model. The C3D8R (8-node linear brick) elements were used to model concrete. Reinforcement bars (steel and GFRP) were modeled as T3D2 truss elements. The loading plate and the support plates were modeled by R3D4 rigid surface elements in ABAQUS to simulate rigid contact surfaces during load transfer and support conditions.

Reinforcement bars were modeled by T3D2 truss elements and embedded in concrete solid elements (C3D8R) using Embedded Region constraint available in ABAQUS. The finite element analysis was performed under the assumption of perfect bond between the concrete and the reinforcement.

The voids of the BubbleDeck are modeled as internal spherical voids inside the concrete body by subtracting the geometry of the voids from the solid part of the concrete. The geometry of concrete slab and the arrangement of the reinforcement were modeled according to the experimental specimen shown in Figure (14). A structured mesh with element sizes varying from 25 mm to 50 mm was utilized in Figure (15), which leads to a good compromise between computational cost and numerical accuracy.

Table 8. CDP parameters values

Parameter	Value
Dilation angle	34°
Eccentricity	0.1
fb0/fc0	1.16
K	0.667
Viscosity	0.0001

4.2 Boundary Conditions and Loading Scheme

The boundary conditions were established to simulate the experimental setup. A full slab model was adopted with simply supported edge conditions using rigid support plates. A concentrated load was applied at the slab center through a rigid loading plate to ensure uniform load distribution. The simply supported boundary conditions were simulated by restraining the vertical displacement (Uz = 0) along the support lines, while additional in-plane restraints (Ux or Uy) were applied at selected locations to prevent rigid body motion without restricting slab rotations.

In the finite element analysis, monotonic loading was applied under displacement-controlled conditions to ensure numerical stability and accurately capture the nonlinear post-cracking response. In contrast, the repeated loading analyses were conducted using force-controlled loading to simulate the experimental loading protocol and repeated loading history adopted in the laboratory tests.

Surface-to-surface contact interactions were defined between the concrete slab and the rigid loading/support plates to ensure proper load transfer. Hard contact behavior was adopted in the normal direction, while a friction coefficient of (0.3) was assigned in the tangential direction. A small viscosity parameter was introduced in the CDP model to improve numerical stability and facilitate convergence during the post-cracking stage of the analysis. The nonlinear analyses were performed using automatic time incrementation in ABAQUS. An initial increment size of 0.005 was adopted, with minimum and maximum increment sizes of 1×10^{-10} and 0.05, respectively.

4.3 Output Parameters

The numerical simulation was verified by the comparison with the test results of some selected specimens. The comparison was made on the key parameters, (the load-deflection behavior, the strength, the reinforcement strain and crack development pattern evolution). The comparison demonstrated that the finite element model provided acceptable agreement with the experimental observations. The specimen 1R-S-M was selected as the reference conventional slab, while specimen 0R-DI-G-D125-M was selected because it represents the most complex configuration investigated in this study, incorporating BubbleDeck voids, GFRP reinforcement, and diaphragm reinforcement. The selected validation specimens were chosen to represent the principal structural configurations investigated in the experimental program. Successful prediction of both specimens provides confidence in the ability of the numerical model to capture the response of the tested slab systems.

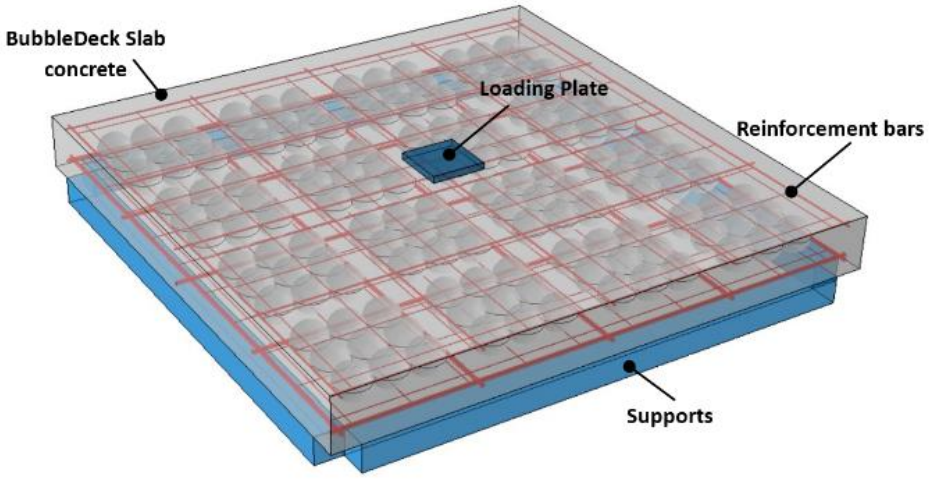

Fig. 14. BubbleDeck slab modeling parts

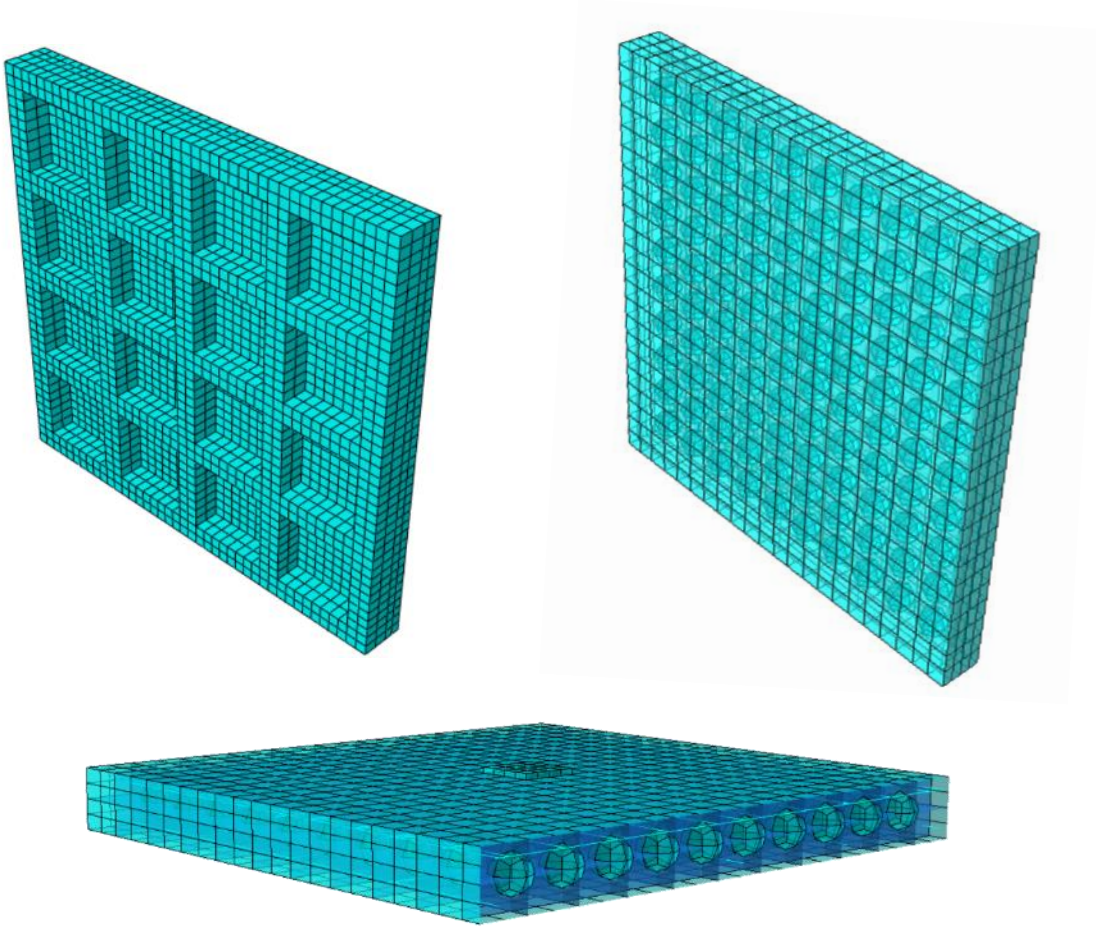

Fig. 15. Ribbed and bubbledeck slabs meshing

4.3.1 Load-Deflection Response

The response of load-deflection predicted by the ABAQUS finite element model was compared with the experimental results, focusing on the initial cracking load, ultimate load, and deflection at ultimate load, as presented in Figure (16) and Table (9). For the control ribbed slab (1R-S-M), the predicted cracking load (44.27 kN) was about 22.4% lower than the experimental value (57.2 kN). However, the predicted ultimate load (230.92 kN) and deflection (13.23 mm) were in close agreement with the experimental findings, with differences of 3.0% and 4.6%, respectively.

For the BubbleDeck specimen (0R-DI-G-D125-M), the predicted cracking load (30.16 kN) differed by 11.5% from the experimental value (34.1 kN). The numerical model overestimated the ultimate load (169.85 kN) and deflection (35.04 mm) compared with the experimental results (147.35 kN

and 30.5 mm). This difference may be attributed to the idealized modeling assumptions adopted in numerical analysis, particularly the perfect bond assumption between the concrete and GFRP reinforcement. As well as the factors of sensitivity of crack initiation to concrete tensile properties, mesh discretization, and the inherent variability associated with concrete cracking behavior.

Table 9. Comparison between experimental and ABAQUS initial cracking load, ultimate loads and deflection for 1R-S-M and 0R-DI-G-D125-M Specimen

Specimen ID	Source	Initial Crack Load (kN)	Difference (%)	Ultimate Load (kN)	Difference (%)	Deflection at Ultimate (mm)	Difference (%)
1R-S-M	Experimental	57.20	-	224.20	-	12.65	-
	ABAQUS	44.27	-22.4	230.92	+3.0	13.23	+4.6
0R-DI-G-D125-M	Experimental	34.10	-	147.35	-	30.50	-
	ABAQUS	30.16	-11.5	169.85	+15.2	35.04	+14.8

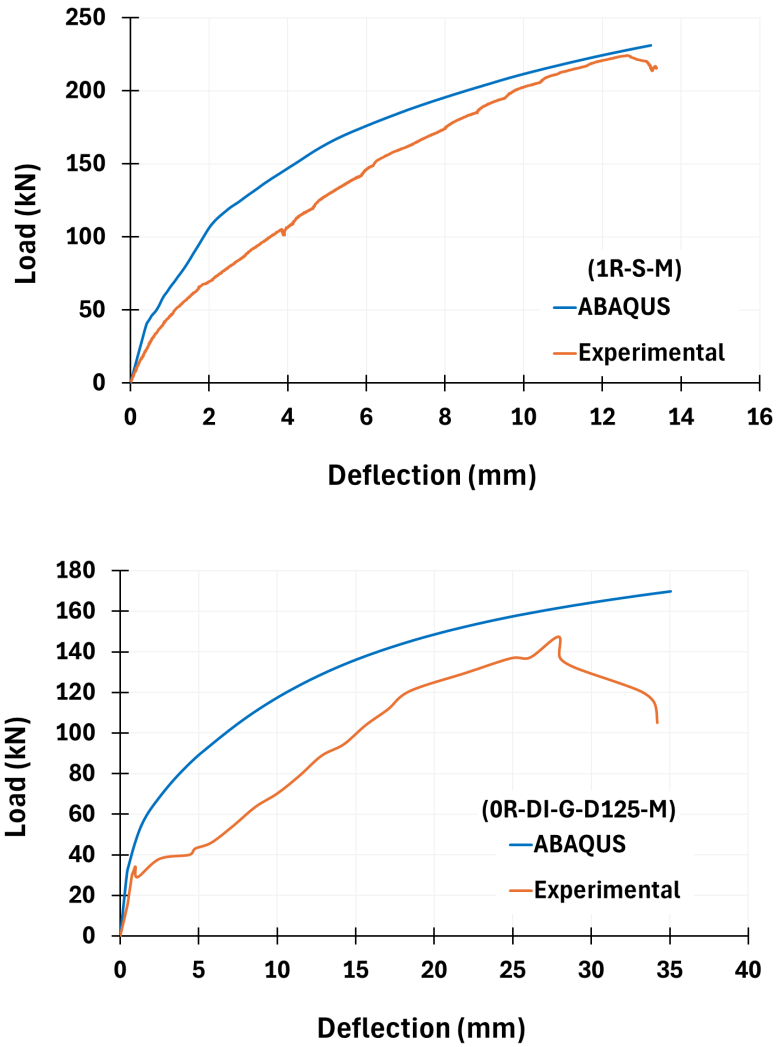

Fig. 16. Experimental and ABAQUS load deflection curves of 1R-S-M and 0R-DI-G-D125-M specimens

4.3.2 Reinforcement Strain

The strain of reinforcement from the result of ABAQUS is compared with the test result in Figure (17). In general, both results exhibit the same tendency, which means that the FE model can accurately reflect the evolution of the reinforcement strain with the load increment.For the control slab (1R-S-M), the numerical and experimental curves display a similar pattern, with strain gradually rising with load. The predicted strain values were somewhat overestimated as compared to the experimental strain values at higher load stages, however the two curves matched well overall.

A similar trend was observed for the BubbleDeck specimen (0R-DI-S-D125-M), although larger differences emerged at higher load levels. The strain predicted by the ABAQUS model was found to overestimate the experimental strain, the difference in strains may be attributed to idealized modeling assumptions such as perfect bond between concrete and reinforcement. Based on the above, it can be concluded that the comparison indicates the ABAQUS model developed can accurately predict the reinforcement strain behavior and the load-strain relationship of the slabs tested.

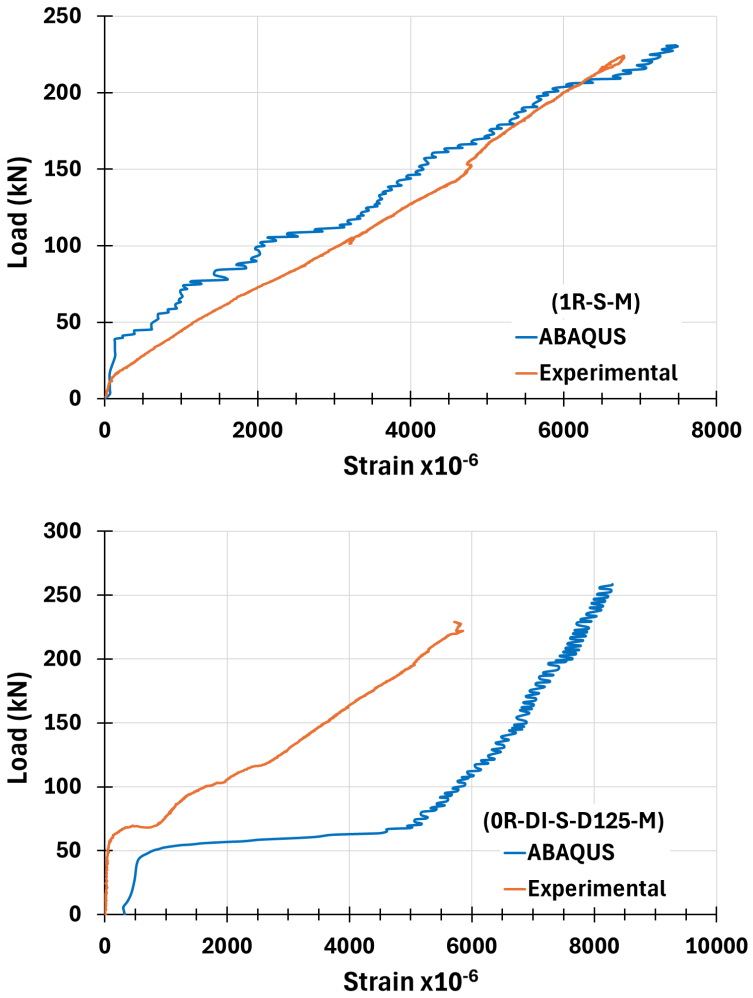

Fig. 17. Experimental and ABAQUS load-strain of bottom bar for 1R-S-M and 0R-DI-S-D125-M specimens

4.3.3 Crack Pattern

Tension crack growth (characterized by the tension damage variable, DAMAGET) in the numerical model was shown by CDP model. In ABAQUS, cracks are modeled by regions where the tensile damage variable is close to one, which indicates that the tensile stiffness is severely degraded. The numerical results reveal that cracks are generated on the slab center and extended radially to the

slab edges as shown in Figure (18). The numerical damage contours exhibited a crack distribution pattern comparable to the experimentally observed cracking behavior, particularly with respect to the radial propagation of cracks and the development of yield-line mechanisms. The validated numerical model is therefore suitable for parametric studies investigating the effects of diaphragm reinforcement ratio and concrete compressive strength on the structural behavior of BubbleDeck slabs.

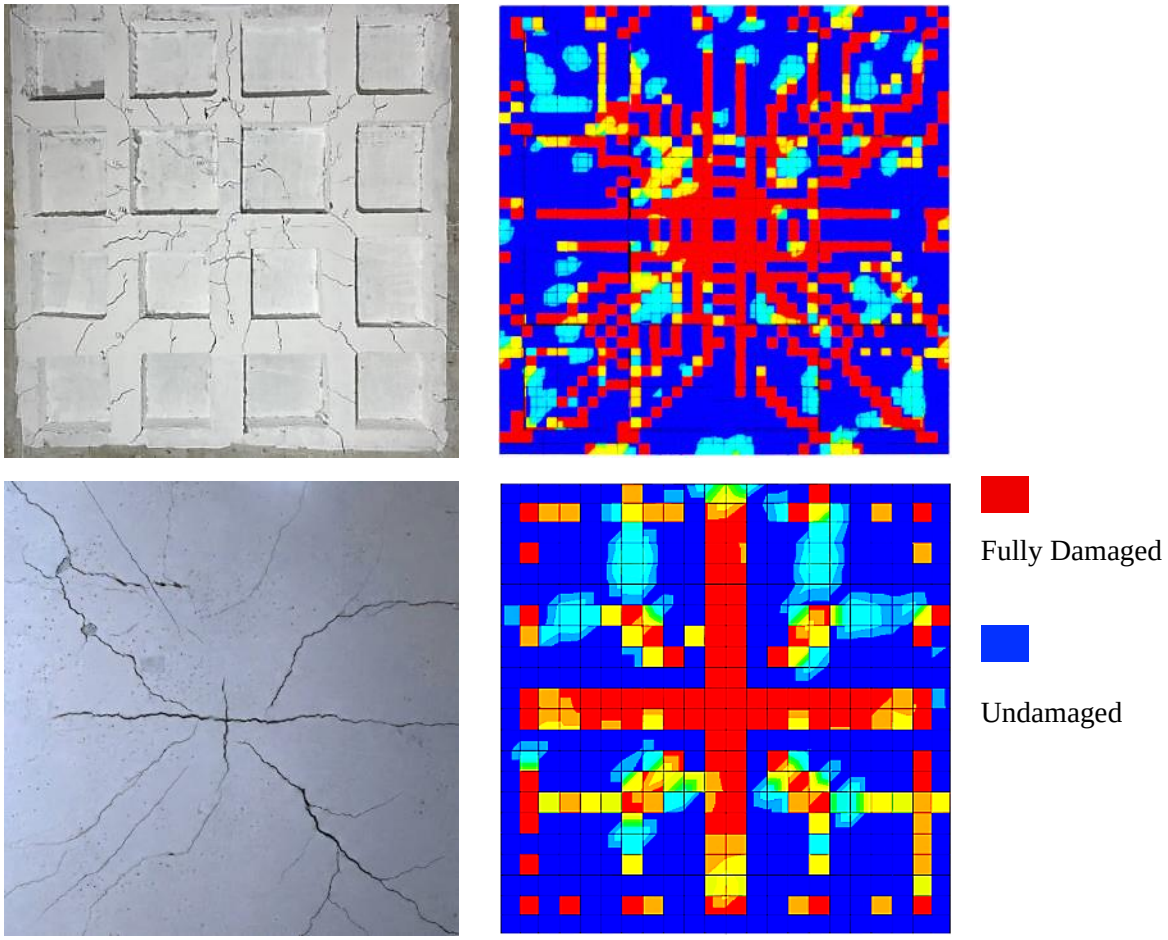

Fig. 18. Crack pattern at ultimate load at bottom face for 1R-S-M and 0R-DI-G-D125-M specimens

4.4. Parametric Study

Following validation of the numerical model against the experimental results, a parametric study was carried out to assess the influence of key design parameters on the structural performance of the BubbleDeck slabs. Two parameters were investigated:

- Diaphragm reinforcement ratio.
- Concrete compressive strength.

4.4.1 Influence of Diaphragm Reinforcement Ratio

This part examines the effects of the diaphragm reinforcement ratio on the behavior of BubbleDeck slab by changing the GFRP reinforcement on the specimen 0R-DI-G-D125-M (1-Φ16, 2-Φ16, 4-Φ16, and 6-Φ16).Results of the numerical study show that an increasing of the diaphragm reinforcement ratio results in a slight increment in the ultimate load capacity. The 1-Φ16 reinforcement configuration accumulated an ultimate load of 169.85 kN, the increase of the reinforcement to 4-Φ16 produced a minor increment in the capacity to 174.65 kN, that is a gain of about of 2.8%. Predicted load-deflection curves shown in Figure (19) illustrated comparable curves in the elastic and post-cracking stages for all reinforcement ratios. Although the GFRP reinforcement ratio was increased; however, its effect on the total flexural stiffness was limited

because the elastic modulus of GFRP bars was relatively low compared to that of concrete section stiffness. Thus, the increase in the quantity of GFRP reinforcement affected only marginally the global flexural stiffness (EI) of the slab system. The increase in ultimate load capacity found was rather minimal which suggests that an increase of the quantity of diaphragm reinforcement may not be an efficient technique for significantly boosting slab capacity. This implies that the amount of reinforcement may not be as important as the placement and layout of the reinforcement.

Hence, the governing parameter in the structural response was the concrete geometry and not the ratio of diaphragm reinforcement. The finite element results confirmed the diminishing gain in the ultimate load capacity beyond the 4Φ16 design. The increase in strength with extra reinforcement was slight and the improvement was small in relation to the increase in the quantity of reinforcement. The 4Φ16 layout is thus the most practicable and cost-effective solution for diaphragm reinforcement for the evaluated loading circumstances as illustrated in Figure (20).

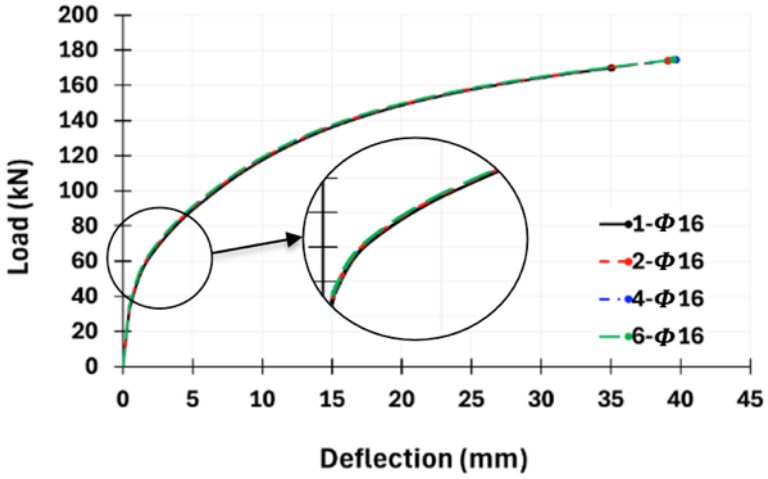

Fig. 19. ABAQUS load deflection curves of 0R-DI-G-D125-M for dfferent GFRP diaphragm reinforcement ratio

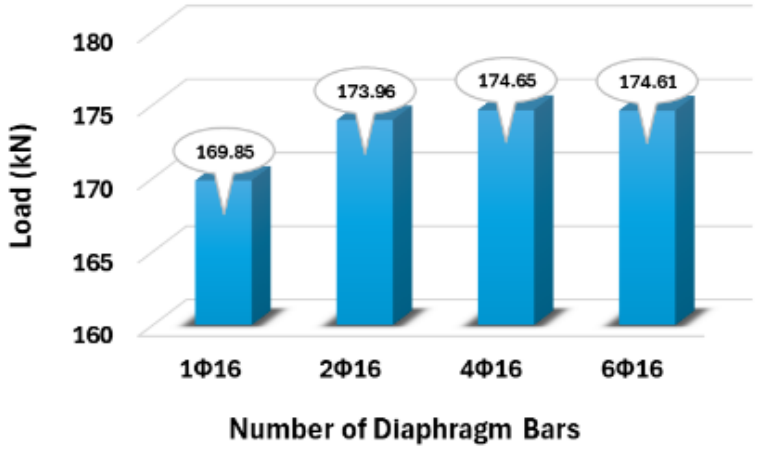

Fig. 20. ABAQUS ultimate load values bar charts of 0R-DI-G-D125-M for different GFRP diaphragm reinforcement ratio

4.4.2 Influence of Concrete Compressive Strength

Since industrial buildings often require high-performance concrete, the numerical model was used to simulate the impact of increasing the compressive strength of concrete around the voids.Four values of compressive strength were considered, (20 MPa, 28 MPa (experimental value), 40 MPa, and 50 MPa). The selected concrete strengths (20, 28, 40, and 50 MPa) reflect a wide range of practical concrete grades used in construction, allowing evaluation of both lower- and higher-

strength concrete on BubbleDeck slab structural performance. The results show that enhancing the compressive strength of concrete significantly improves the load-carrying capacity of the slab as shown in Figures (21) and (22). For instance, increasing the compressive strength from 28 MPa to 50 MPa resulted in an increase in ultimate load from 169.85 kN to 238.45 kN, corresponding to an increase of approximately 40%.

Although the slabs were designed as under-reinforced members, the increase in concrete compressive strength enhanced not only the compressive zone capacity but also the stiffness and load-transfer capability of the concrete ribs between the voids. Consequently, the influence of concrete strength on the ultimate load was more pronounced than typically observed in conventional solid reinforced concrete members. The results also show that higher concrete strength leads to slightly larger ultimate deflections due to the increased load capacity before failure. The increase in concrete compressive strength also resulted in a steeper initial slope of the load-deflection curves, indicating higher initial stiffness. However, the corresponding increase in ultimate load capacity allowed the slabs to sustain larger ultimate deflections before failure.

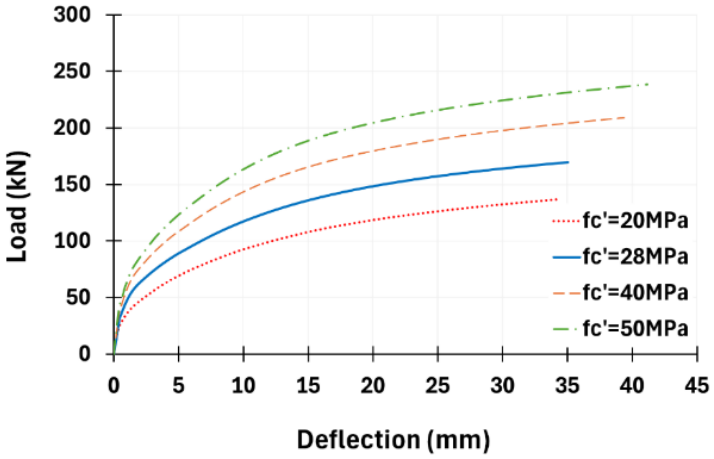

Fig. 21. ABAQUS load deflection curves of 0R-DI-G-D125-M for different concrete compressive strength

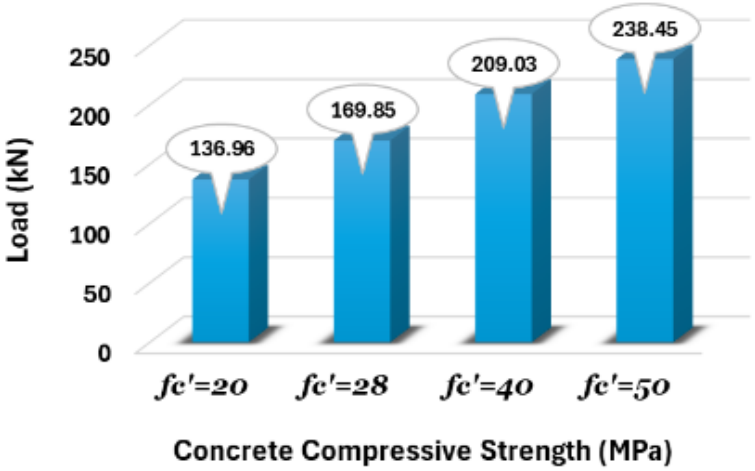

Fig. 22. ABAQUS ultimate load values bar charts of 0R-DI-G-D125-M for different concrete compressive strength

5. Design Implications for GFRP-Reinforced BubbleDeck Slabs

The findings of the present experimental and numerical investigation provide several important insights for the design and practical implementation of GFRP-reinforced BubbleDeck slab systems.First, the experimental results confirm that the structural behavior of BubbleDeck slabs is primarily governed by two-way flexural action. The crack patterns observed in all specimens

initiated at the slab center and propagated radially toward the slab edges, forming typical yield-line mechanisms. This indicates that the structural response of BubbleDeck slabs can be reasonably analyzed using classical two-way slab theory combined with yield-line concepts.

Second, the comparison between steel-reinforced and GFRP-reinforced specimens revealed significant differences in stiffness and deformation behavior. Steel-reinforced slabs were stiffer and sagged less, due to the larger modulus of elasticity of steel reinforcement. Meanwhile, Slabs reinforced with GFRP bars experienced more deflections and crack spacing. For GFRP-reinforced BubbleDeck slabs, serviceability requirements related to deflection and crack width should govern the design process. The provisions of ACI 440.1R should therefore be carefully considered when selecting reinforcement ratios and slab dimensions to ensure acceptable service performance.

The slabs showed significant deformation and progressive crack growth before failure, despite GFRP reinforcement's brittle rupture mechanism. The structure did not collapse suddenly, and massive deflections and apparent crack propagation warned of failure. Therefore, GFRP reinforcement may be considered a feasible substitute for steel reinforcement in BubbleDeck slab systems, especially in applications where corrosion resistance is needed.

The ultimate bearing capacity was found to be increased by the improvement in the compressive strength of the concrete. This indicate that the concrete compressive strength has a notable influence in counteracting the flexural stresses induced in BubbleDeck slabs. According to the experimental and numerical findings, the following design suggestions are given:

- For BubbleDeck slabs reinforced with GFRP bars, particular attention should be given to serviceability requirements. Increasing the reinforcement ratio or slab depth may be necessary to compensate for the lower elastic modulus of GFRP bars and to limit deflections under service loads.
- From a design perspective, increasing concrete compressive strength appears to be a more effective strategy for enhancing the structural performance of GFRP-reinforced BubbleDeck slabs than simply increasing the diaphragm reinforcement ratio. Therefore, the use of higher-strength concrete may provide a practical means of improving stiffness and load-carrying capacity while maintaining the advantages of GFRP reinforcement.
- The adopted FEM analysis presented in this paper can be used as an effective instrument to predict the structural behavior of BubbleDeck slabs at the design stage.

Overall, the integration of GFRP reinforcement and BubbleDeck slab technology provides a promising structural solution for lightweight, sustainable, and durable floor systems in modern construction.

6. Conclusions

The structural behavior of GFRP-reinforced biaxial voided slabs (BubbleDeck slabs) was explored by experimental testing and nonlinear finite element analysis utilizing ABAQUS with the Concrete Damaged Plasticity (CDP) model. The primary findings from testing twelve slab specimens are as follows:

- The typical two-way flexural behavior was observed in all tested slabs, and the cracking was initiated under the load and propagated radially to the margins of the slab. The failure mechanism was mainly dominated by flexural action and yield-line development.
- The type of reinforcement had a considerable effect on the responsiveness of the slab. The higher elastic modulus of the steel reinforcement resulted in higher stiffness and lower deflections of the steel-reinforced slabs, and larger deformability and broader crack distribution of the GFRP-reinforced slabs with stable structural behavior up to failure.
- The investigated BubbleDeck configuration achieved a concrete volume reduction of approximately 18.5% while maintaining adequate structural performance, demonstrating the potential of biaxial voided slabs to reduce material consumption and self-weight.
- The structural performance and load carrying capacity of BubbleDeck slabs with GFRP bars as reinforcement were maintained even with the reduced concrete volume due to the

spherical voids. This indicates the viability of using GFRP reinforcement in lightweight biaxial slab systems.

- The effect of diaphragm reinforcement was dependent on the type of reinforcement. The load redistribution features, and the ultimate load capacity were enhanced with the diaphragm configuration in steel-reinforced slabs. However, improvements in fracture dispersion and stress redistribution did not lead to a comparable gain in ultimate load capacity of the GFRP-reinforced slabs.
- The two types of slabs exhibited increasing stiffness deterioration and spreading of cracks under repeated loading. However, the primary failure mode was still flexural, without abrupt instability in the loading cycles.
- The finite element models created in this work reasonably described the overall structural response of the tested slabs such as load-deflection behavior, reinforcement strain and crack patterns. The disparity between the experimental and numerical results was deemed acceptable because of the idealized assumptions used in the numerical simulation.
- The increase of concrete compressive strength greatly improved the structural performance and ultimate load capacity of the BubbleDeck slabs, which indicates the critical contribution of concrete strength to the flexural resistance of voided slab systems.
- The application of BubbleDeck technology with GFRP reinforcement offers a promising sustainable structural solution due to the simultaneous reduction in concrete consumption and the removal of corrosion-related deterioration associated with conventional steel reinforcement. Such solutions can help in reducing the structural self-weight, increase the service life and reduce the maintenance requirements especially in harsh situations such as maritime and coastal constructions.
- Further research is suggested for the assessment of long-term fatigue behavior, environmental durability and serviceability performance of the GFRP-reinforced BubbleDeck slabs under realistic field stress circumstances.

Acknowledgement

Acknowledgment is made to the Department of Civil Engineering at the University of Mosul for providing the necessary laboratory facilities and academic support that significantly enhanced the findings of this research project.

References

[1] Alnemrawi BR, Al-Rousan RZ, Ababneh AN. CFRP strengthening for improving punching shear of heat-damaged flat slabs with openings. Engineering Failure Analysis . 2024;160:108208. https://doi.org/10.1016/j.engfailanal.2024.108208

[2] Alrousan RZ, Alnemrawi BR. Punching shear of FRP reinforced concrete slabs under varying configurations and loading. Case Studies in Construction Materials. 2022;17:e01508. https://doi.org/10.1016/j.cscm.2022.e01508

[3] Oukaili N, et al. Reduced volume approach for evaluating punching shear resistance in biaxial bubbled slabs. Buildings. 2024;14(3):1-26. https://doi.org/10.3390/buildings14030676

[4] Abdul Aziz Z, Heng CL. Bubble deck slab system: review on design and performance. International Journal for Innovation Education and Research. 2021;9(9):575-588. https://doi.org/10.31686/ijier.vol9.iss9.3397

[5] Sivagamasundari R, Kumaran G. Flexural behaviour of one-way concrete slabs reinforced with GFRP vs conventional bars. The Open Civil Engineering Journal. 2008;2:24-34. https://doi.org/10.2174/1874149500802010024

[6] Sonia BM, Vijay Kumar YM. Review on bubble deck slab technology. International Journal of Multidisciplinary Educational Research. 2021;10(4):65-67.

[7] Khouzani SM, et al. Numerical study on flexural behavior of biaxial voided slabs with steel cages. Journal of Building Engineering. 2021;44. https://doi.org/10.1016/j.jobe.2021.103382

[8] Gajewski T, et al. Optimal design of bubble deck concrete slabs: Serviceability limit state. Materials. 2023;16(14):1-17. https://doi.org/10.3390/ma16144897

[9] Mahdi MSD, et al. Bubbles distribution influence in BubbleDeck slab under harmonic loading: Experimental/numerical analysis. Engineering, Technology & Applied Science Research. 2021;11(1):6645-6649. https://doi.org/10.48084/etasr.3963

[10] Ye L, Feng P, Yue Q. Advances in FRP Composites in Civil Engineering. Proceedings of the 5th International Conference on FRP Composites in Civil Engineering (CICE 2010), Sep 27-29, 2010, Beijing, China. https://doi.org/10.1007/978-3-642-17487-2
[11] Tu J, Zhao Q, Gao K. Design of GFRP reinforced concrete beams based on crack width. Materials 2022;15(18):1-18. https://doi.org/10.3390/ma15186467
[12] Mohammed AD, Salih OA. Experimental study on RC beams with GFRP and steel bars under flexure strength properties. Civil and Environmental Engineering. 2025;21(1):282-298. https://doi.org/10.2478/cee-2025-0022
[13] Mutashar BM, et al. Structural behavior of beam-column connection using post-installed steel and GFRP rebars. Civil Engineering Journal. 2026;12(2):563-578. https://doi.org/10.28991/CEJ-2026-012-02-08
[14] Ashour AF. Flexural and shear capacities of concrete beams reinforced with GFRP bars. Construction and Building Materials. 2006;20(10):1005-1015. https://doi.org/10.1016/j.conbuildmat.2005.06.023
[15] Benmokrane B, et al. Flexural response of concrete beams reinforced with FRP bars. ACI Structural Journal. 1996;93(1):46-55. https://doi.org/10.14359/9839
[16] Barris C, et al. Cracking and deflections in GFRP RC beams: experimental study. Composites Part B: Engineering. 2013;55:580-590. https://doi.org/10.1016/j.compositesb.2013.07.019
[17] Mutashar B M, Kasim S Y, Salih O A. Experimental evaluation of bond behavior of post-installed GFRP and steel reinforcements using different adhesives. Research on Engineering Structures & Materials, 2026; 12(2): 1055-1066. https://doi.org/10.17515/resm2026-1246ic1012rs
[18] S. H. Mtashar and A. A. Al-Azzawi. Finite Element Analysis of Voided Reinforced Concrete Slabs Enhanced by GFRP Sheets under Monotonic and Repeated Loads. Journal of Engineering,2024, 30(10):46-68. https://doi.org/10.31026/j.eng.2024.10.04
[19] Sidhardhan JS, Madasamy M. The structural performance of slab reinforced with steel and GFRP bars subjected to static and static cyclic load. Revista. Matéria. 2024;29(4):e20240172. https://doi.org/10.1590/1517-7076-rmat-2024-0172
[20] Al-shaarbaf I, Ali A, Ahmed M. Influence of loading pattern regime on behavior of self-compacting concrete voided slab strips under repeated load. Engineering and Technology Journal. 2020;38(7):967-974. https://doi.org/10.30684/etj.v38i7A.458
[21] Lubliner J, et al. A plastic-damage model for concrete. International Journal of Solids and Structures. 1989;25(3):299-326. https://doi.org/10.1016/0020-7683(89)90050-4
[22] Lee J, Fenves GL. Plastic-damage model for cyclic loading of concrete structures. ASCE Journal of Engineering Mechanics. 1998;124(8):892-900. https://doi.org/10.1061/(ASCE)0733-9399(1998)124:8(892)
[23] Mohammed Ali AA, Al-Darzi SY. Sustainable behavior of GFRP-reinforced bubble deck slabs: Experimental approach. Asian Journal of Civil Engineering. 2026;27(5):2301-2314. https://doi.org/10.1007/s42107-025-01616-0
[24] American Concrete Institute. ACI 211.1-22 - Standard Practice for Selecting Proportions for Normal, Heavyweight, and Mass Concrete. 2022.
[25] Iraqi Standard Specification. Properties of ordinary Portland cement (No. 5). Iraq; 2018.
[26] BSI. BS 882: Specification for aggregates from natural sources for concrete. BSI, 1992.
[27] ASTM International. ASTM C143/C143M - Standard Test Method for Slump of Hydraulic-Cement Concrete. West Conshohocken, PA, 2022.
[28] ASTM D7205. Standard test method for tensile properties of FRP bars. ASTM International; 2016.
[29] ASTM D7957. Standard specification for solid round GFRP bars for concrete reinforcement. ASTM International; 2022.
[30] Al-Saffar IS. Nonlinear analysis for composite steel-concrete beam elements under repeated load, MSc Thesis, University of Mosul, 2006.
[31] Al-Haj Ahmed KA. Investigating the effect of repeated loads on the behavior of steel-concrete composite bridge joints, PhD Thesis, University of Mosul, 2022.
[32] American Concrete Institute. ACI 440.11-22 - Building Code Requirements for Structural Concrete Reinforced with Glass Fiber-Reinforced Polymer (GFRP) Bars-Code and Commentary. 2022.